Geochimica et Cosmochimica Acta 399 (2025) 93–110

Contents lists available at ScienceDirect

Geochimica et Cosmochimica Acta

journal homepage: www.elsevier.com/locate/gca

Dissolved zinc and cadmium isotope systematics in the Amundsen and Weddell coastal Antarctic marginal seas

Hung-An Tian [a], Mathijs van Manen [a], Charlotte Eich [b,c], Jinyoung Jung [d], Willem H.v.d. Poll [e], Gert-Jan Reichart [a,f], Tim M. Conway [g], Rob Middag [a,e,*]

[a] Department of Ocean Systems, NIOZ Royal Netherlands Institute for Sea Research, 1790 AB Den Burg, the Netherlands
[b] Department of Marine Microbiology and Biogeochemistry, NIOZ Royal Netherlands Institute for Sea Research, 1790 AB Den Burg, the Netherlands
[c] Institute for Biodiversity and Ecosystem Dynamics, University of Amsterdam 1098 XH Amsterdam, the Netherlands
[d] Korea Polar Research Institute, 26, Songdomirae-ro, Yeonsu-gu, Incheon 21990, Republic of Korea
[e] Centre for Isotope Research - Oceans, University of Groningen 9700 AB Groningen, the Netherlands
[f] Department of Geosciences, Utrecht University, 3584 CB Utrecht, the Netherlands
[g] College of Marine Science, University of South Florida, FL 33701 St Petersburg, USA

ARTICLE INFO

Associate Editor: Yoshiki Sohrin

Keywords:
GEOTRACES
Trace metals
Isotope compositions
Biogeochemistry

ABSTRACT

Coastal Antarctica is experiencing rapid environmental change with potential effects on regional marine trace element biogeochemistry. Here, we investigate the biogeochemistry of two dissolved bioactive trace elements, zinc (Zn) and cadmium (Cd), and their isotope ratios (δ^{66}Zn and δ^{114}Cd) in two coastal marginal seas with distinct oceanographic features – the Amundsen Sea with the intrusion of Circumpolar Deep Water (CDW) onto the Antarctic continental shelf, and the Weddell Sea where formation of Antarctic Bottom Water occurs. In the Amundsen Sea, our isotope data show CDW predominantly controls δ^{66}Zn and δ^{114}Cd on the continental shelf. This result is consistent with previous concentration-focused studies that suggested only a negligible addition of Zn and Cd from continental sediments and ice shelf meltwater, and other processes (e.g., scavenging) play a limited role in their cycling on the shelf region. In the Weddell Sea, homogeneous δ^{66}Zn and δ^{114}Cd within different water masses across the Antarctic Peninsula shelf, while Zn and Cd concentrations increase via physical mixing with deep water masses, suggest a preformed isotope signature on the continental shelf. In surface waters of both regions, δ^{114}Cd exhibited isotope fractionation linked to biological uptake, with different Rayleigh closed system fractionation factors ($\alpha = R_{biomass}/R_{seawater}$) for regions dominated by haptophytes (0.99930–0.99960) and diatoms (0.99970–0.99995) and we speculate that such differences may be associated with variability between species. In contrast, estimated fractionation factors for Zn in haptophytes (0.99995) and diatoms (0.99980–0.99995) dominated blooms are similar and comparable to reported values in the Southern Ocean (0.99995 ± 0.00001). At the intermediate depth (250–1500 m) in the Weddell Sea, significantly lower δ^{114}Cd in the inner gyre compared to the outer gyre implies Cd regeneration and reduced ventilation. This pattern was not observed for δ^{66}Zn, likely due to its smaller biological fractionation in the surface. These findings confirm the role of CDW as the main source of Zn and Cd to the Amundsen Sea and the importance of physical mixing in setting global dissolved Zn and Cd distributions during the formation of deep waters in the Weddell Sea, providing insights into the impacts of regional coastal systems on the biogeochemistry of Zn and Cd.

1. Introduction

Marine phytoplankton significantly influence global climate through photosynthesis and their role in the marine carbon cycle (Field et al., 1998; Martin et al., 1990). Besides macronutrients like phosphate, nitrate, and silicate, micronutrients such as zinc (Zn) are essential for phytoplankton metabolism. Zn is the second most abundant micronutrient in phytoplankton (Twining and Baines, 2013) necessary for enzymes involved in carbon fixation and phosphate acquisition (Morel et al., 1994; Shaked et al., 2006). Although cadmium (Cd) is considered toxic, some marine algae use Cd to replace Zn for carbonic anhydrase (e.g., Park et al., 2007; Price and Morel, 1990; Sunda and Huntsman,

* Corresponding author.
E-mail addresses: hung-an.tian@nioz.nl (H.-A. Tian), rob.middag@nioz.nl (R. Middag).

https://doi.org/10.1016/j.gca.2025.04.017
Received 14 July 2024; Accepted 18 April 2025
Available online 20 April 2025

1995). Consequently, dissolved Zn (dZn) and Cd (dCd) show nutrient-like distributions similar to silicate (SiO_2) and phosphate (PO_4) in the oceans (e.g., Bruland, 1980). Specifically, the vertical profile of dZn appears more closely correlated to SiO_2, whereas dCd is more closely coupled with PO_4 (Bruland et al., 2014). These differences are thought to be driven by differences in the effects of biogeochemical processes and subsequent mixing with waters from high latitude regions such as the Southern Ocean and the North Atlantic Ocean featured with distinct elemental ratios in playing a key role in the coupling of these micro- and macronutrients (Middag et al., 2019; Middag et al., 2018; Vance et al., 2017; Weber et al., 2018). As such, a detailed understanding of the cycling and distribution of Zn and Cd in the Southern Ocean is needed.

Oceanic dissolved Zn and Cd isotope ratios (δ^{66}Zn and δ^{114}Cd) can improve our understanding of their marine biogeochemistry and cycling (Conway et al., 2021; Horner et al., 2021; Schlitzer et al., 2018). In deep waters sourced from the Southern Ocean, δ^{66}Zn is relatively homogeneous at + 0.44 ± 0.08 ‰ (mean ± 2 SD) (e.g., Bermin et al., 2006; Conway and John, 2014; Lemaitre et al., 2020; Sieber et al., 2020; Sieber et al., 2023; Takano et al., 2017), similarly, δ^{114}Cd averages + 0.25 ± 0.06 ‰ (e.g., Abouchami et al., 2014; Conway and John, 2015; George et al., 2019; Sieber et al. (2023); Xie et al., 2017; Xie et al., 2019; Yang et al., 2012).

In the surface ocean, δ^{114}Cd is commonly influenced by biological uptake, which preferentially absorbs light Cd isotopes, resulting in a heavy isotope signature in seawater of up to ~+1 to + 5 ‰ (e.g., Abouchami et al., 2011; Conway and John, 2015; Janssen et al., 2019; John and Conway, 2014; John et al., 2018; Lacan et al., 2006; Ripperger et al., 2007; Xue et al., 2013; Yang et al., 2018). This effect is prominent in the Southern Ocean, where nutrients in surface waters are only partially utilized. Here, upwelling of nutrient-rich upper Circumpolar Deep Water (CDW) in the Antarctic Zone (AZ) supports phytoplankton growth, creating an isotopically heavy dCd pool in Antarctic Surface Water. This signature is then transported north by Subantarctic Mode Water (SAMW) and Antarctic Intermediate Water (AAIW) into the Atlantic Ocean (Abouchami et al., 2014; Conway and John, 2015; Xie et al., 2017) and the Pacific Oceans (Sieber et al., 2019; Sieber et al. (2023)). The imprint of these Antarctic processes underscores the Southern Ocean's influence on global δ^{114}Cd distributions. While biological uptake and circulation are key factors, other processes like ligand complexation (Gault-Ringold et al., 2012; George et al., 2019; Ratié et al., 2021; Xie et al., 2017), shallow remineralization (Sieber et al., 2019; Xue et al., 2013), and external Cd sources (Cloquet et al., 2006; Lambelet et al., 2013; Schmitt et al., 2009; Sieber et al., 2023; Yang et al., 2015) may also affect surface δ^{114}Cd.

For dissolved δ^{66}Zn, the surface pattern is much less clear, with values from ~ –0.20 to ~+0.90 ‰, contrasting culturing experiments showing preferential uptake of light Zn isotopes (John and Conway, 2014; John et al., 2007; Köbberich and Vance, 2017; Samanta et al., 2018). Several processes are proposed to explain this variability. Ligand complexation, such as with EDTA, might mask the uptake of light Zn isotopes (e.g., Köbberich and Vance, 2019). Adsorption tends to favor heavy Zn isotopes, indicating that reversible scavenging could influence surface δ^{66}Zn (Grun et al., 2023; John and Conway, 2014; Sieber et al. (2019); Weber et al., 2018). Shallow remineralization also contributes to a lighter dZn pool (Bermin et al., 2006; Ellwood et al., 2020; Wang et al., 2019; Zhao et al., 2014), and light Zn from sedimentary and hydrothermal sources might impact surface δ^{66}Zn as well (Conway and John, 2014; Lemaitre et al., 2020). Consequently, this interplay results in variable surface δ^{66}Zn, which also varies regionally. For example, surface Southern Ocean values generally match deep ocean δ^{66}Zn values (Sieber et al., 2020; Wang et al., 2019; Zhao et al., 2014), whereas low-latitude regions show more variability (Conway and John, 2014, 2015; John et al., 2018; Lemaitre et al., 2020; Liao et al., 2020; Vance et al., 2019). A comprehensive investigation of δ^{66}Zn across multiple Southern Ocean zones by Sieber et al. (2020) showed that the uptake of Zn results in a small apparent fractionation in AZ and δ^{66}Zn continually increases via uptake as the surface waters move towards Polar Frontal Zone. However, unlike for Cd, where the subduction of SAMW and AAIW carrying elevated δ^{114}Cd influences the lower-latitude water column, SAMW and AAIW only carry a relatively small amount of dZn – which is also only slightly isotopically heavier than deep water – and so these water masses are not believed to act as a significant lever on subsurface Zn isotope compositions at lower latitudes (Sieber et al., 2020).

The current study focuses on two different coastal Antarctic regions – the Amundsen Sea and the Weddell Sea. In the Amundsen Sea, warm modified Circumpolar Deep Water (mCDW) intrudes onto the continental shelf, driving rapid ice sheet melt beneath ice shelves (Dutrieux et al., 2014; Gourmelen et al., 2017; Jacobs et al., 2012; Jacobs et al., 1996; Kim et al., 2021; Miles et al., 2016; Wåhlin et al., 2013). Upwelled mCDW also accelerates sea ice melt, creating highly productive polynyas during the spring-summer period (Arrigo and van Dijken, 2003; Yager et al., 2012). The Amundsen Sea Polynya has the highest rate of annual net primary production among Antarctic polynyas, (Arrigo et al., 2012; Arrigo and van Dijken, 2003; Yager et al., 2012), likely due to additional dissolved Fe input from Fe-rich mCDW and particulate Fe input from ice shelf melting relieving Fe-limitation (Gerringa et al., 2012, 2020; Planquette et al., 2013; Sherrell et al., 2015; Tian et al., 2023; van Manen et al., 2022). To date, only a few studies have investigated dissolved concentrations of both elements in these regions. In the Amundsen Sea, mCDW is considered the primary source of dZn (up to 7 nmol L^{-1}) and dCd (up to 0.75 nmol L^{-1}), with minor contributions from sediments and no significant input from ice shelf meltwater (Sherrell et al., 2015; Tian et al. (2023)). Observations from those studies were based solely on dissolved and particulate concentrations – dissolved isotope composition, a powerful proxy for tracing sources and biogeochemical processes, have not yet been made available in this region.

On the other side of the continent, the Weddell Sea situated in the western part of the predominantly wind-driven cyclonic Weddell Gyre is crucial for global deep-water formation (Orsi et al., 1999; Orsi et al., 2002). In the southern and western Weddell Sea, extensive sea ice formation with brine rejection facilitate dense, saline, and cold shelf water formation that descends along the continental slope, eventually contributing a significant portion of equatorward flowing Antarctic Bottom Water (AABW) as it exits through the Scotia Sea (Jullion et al., 2014; Orsi et al., 1999; Orsi et al., 2002; Vernet et al., 2019). As such, the Weddell Sea plays a critical role in global climate and global thermohaline circulation (Fahrbach et al., 1994; Foldvik et al., 1985; Marinov et al., 2006), and potentially global nutrient cycling. Compared to the Amundsen Sea, greater efforts have been made to investigate dZn and dCd in the Weddell Sea (Baars et al., 2014; Baars and Croot, 2011; Croot et al., 2011; Nolting and de Baar, 1994; Nolting et al., 1991; Westerlund and öhman, 1991). In the western Weddell Sea, Sañudo-Wilhelmy et al. (2002) reported increasing surface [dZn] and [dCd] from the open Weddell Sea toward the coast, suggesting that ice melt, upwelling, and sediment resuspension enrich nearshore waters, highlighting the importance of coastal input. In the eastern Weddell Sea (Zero Meridian), the highest [dZn] (6–7 nmol L^{-1}, Croot et al., 2011) and [dCd] (~0.86 nmol L^{-1}, Baars et al., 2014) are observed in Warm Deep Water (WDW), among other deep waters (i.e., Weddell Sea Deep Water and Weddell Sea Bottom Water), associated with the transport of CDW (high [dZn] and [dCd]) from Antarctic Circumpolar Current. In contrast to concentration data, δ^{114}Cd measurements in the Weddell Sea remain scarce. Abouchami et al. (2014) and Abouchami et al. (2011) presented vertical profiles of δ^{114}Cd near the Zero Meridian, while Xue et al. (2013) presented δ^{114}Cd profiles from two stations in the western Weddell Gyre near the Antarctic Peninsula. The lack of δ^{114}Cd coverage across the section toward the central Weddell Gyre limits our understanding of Cd cycling in this region.

Given the diverse characteristics of the Amundsen Sea and the Weddell Sea, as well as the biogeochemical functions of Zn and Cd, it is conceivable that both regions may exhibit spatial variability in the cycling and distribution of both elements, with potential impacts at the

global scale (e.g., do biogeochemical processes in coastal Antarctic region 'set' the isotope signatures for AABW?). Our aim is to use isotope compositions to assess external sources in the Amundsen Sea and investigate the marine cycling of these elements in the western Weddell Sea, as well as the biogeochemical processes affecting isotope variability in Antarctic waters. Consequently, the data presented in this study provides further implications on how changing coastal Antarctica influences the biogeochemical cycling of Zn and Cd in the Southern Ocean.

2. Materials and methods

2.1. Shipboard sampling

Two GEOTRACES process studies (ID-expedition: GPpr12-ANA08B and GApr12-PS117) were conducted onboard the Korean icebreaker R/V Araon and German icebreaker R/V Polarstern (AWI, 2017) during Austral Summer (December 2017 to February 2018 in the Amundsen Sea and December 2018 to February 2019 in the Weddell Sea), respectively. Several relevant trace metal studies from ANA08B are published for dissolved and particulate Cd and Zn concentrations (Tian et al. (2023)), dissolved Fe and Mn (van Manen et al., 2022) and dissolved Fe isotope composition (Tian et al., 2023), from which the sampling procedures have been described. The primary difference in terms of sampling between the two expeditions was the filter used – AcroPak-400 filters (VWR, precleaned with HCl and stored in MQ) were used in the Weddell Sea, while Sartobran-300 filters (Sartorius, rinsed with MQ) were used in the Amundsen Sea.

For the ANA08B expedition, filtered seawater samples (1 and 4 L, with 4 L for near-surface samples) were collected in the Amundsen Sea (71-74°S, 112-128°W) along two transects – the Dotson Ice Shelf (DIS) transect (10 stations: Stns 53, 52, 50, 49, 48, 45, 42, 36, 34, 33) and the Getz Ice Shelf (GIS) transect (3 stations: Stns 55, 24, 57), representing the pathways of modified Circumpolar Deep Water (mCDW) inflow and outflow. In this study, and as previously described (Tian et al., 2023b), stations were grouped by location – open ocean station (Stn 53), off-shelf station (Stn 55), shelf break stations (Stns 52, 24), mCDW inflow stations (Stns 50, 49, 48, 45, 42), and mCDW outflow stations (Stns 36, 34, 33) (Fig. 1).

For the PS117 expedition, seawater samples (1 and 4 L) were collected along a transect in the western Weddell Sea (63-66°S, 36-54°W, Fig. 1). The 12 stations were grouped into the shelf stations (Stns 95, 93, 91), continental slope stations (Stns 82, 85, 75, 73, 70, 67), and off-shore stations (Stns 65, 61, 56) (Fig. 1).

2.2. Sample processing for δ^{66}Zn and δ^{114}Cd analysis

All seawater samples were acidified onboard to pH ~ 1.8 using 0.024 M HCl inside an ISO class-5 laminar flow hood, following the procedure for concentration samples (Tian et al., 2023b; van Manen et al., 2022). The samples were then transported to the clean room (ISO class 7, ISO class 5 in working hoods) at the Royal Netherlands Institute for Sea Research (NIOZ) for further processing. All water and reagents used were ultrapure water (MQ, <18.2 MΩ cm^{-1}) and of ultrapure quality, respectively (Tian et al., 2023; Tian et al., 2023b).

Filtered seawater samples were processed using a modified method (i.e., extraction and purification) modified from Conway et al. (2013) and Sieber et al. (2019a), and have been described in detail by Tian et al. (2023a) and Supplementary Table S1, which was validated (i.e., procedural blank and recovery) for Zn and Cd isotope analysis (see Supplementary Fig. S1 for details) prior to processing natural samples.

2.3. Double spike technique and analysis by Multi-Collector ICPMS (MC-ICPMS)

Zn and Cd isotope analysis were carried out using a double-spike technique on a Thermo Neptune Plus Multi-collector ICPMS (MC-ICPMS) at NIOZ (Siebert et al., 2001), following a modified procedure (Supplementary S2 and Table S1). Seawater samples were spiked with ^{64}Zn-^{67}Zn and ^{111}Cd-^{113}Cd double spikes (see Supplementary S1) with a sample-to-spike ratio of 1:1 (Sieber et al., 2019a, 2020), at least 48 h prior to further treatments, guided by dissolved concentrations measured independently by a SeaFAST system and ICP-MS as reported previously (Tian et al., 2023b; van Manen et al., 2022).

Here, we express Zn and Cd isotope ratios in typical delta notations

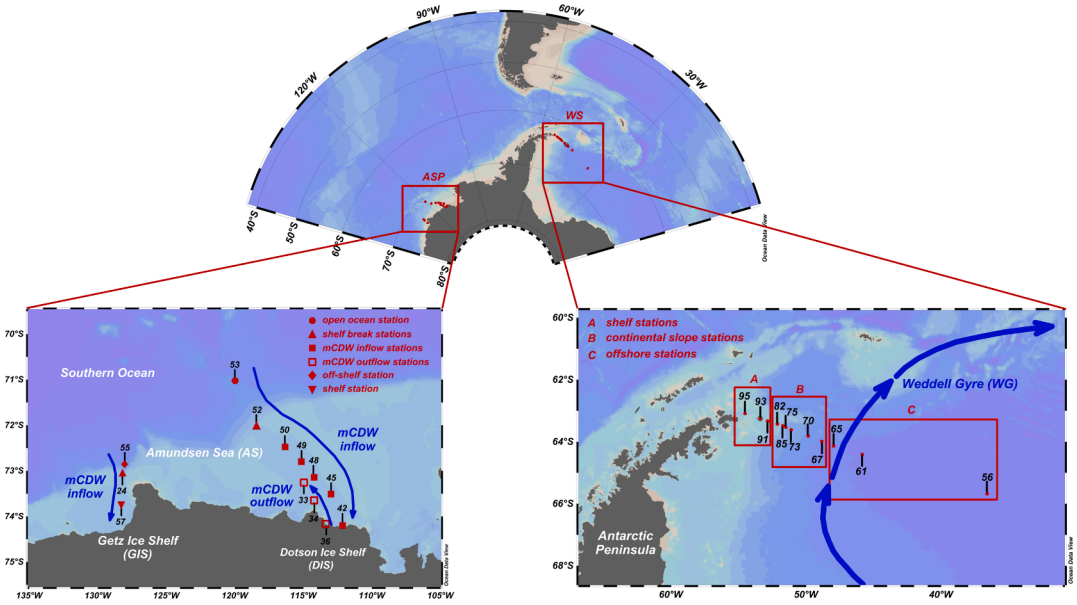

Fig. 1. Sampling stations of expedition ANA08B (the Amundsen Sea) and PS117 (the Weddell Sea). Samples were collected during Austral Summer (December 2017 to February 2018 and December 2018 to February 2019), respectively. Expedition ANA08B comprised two transects – the DIS transect (Stns 53, 52, 50, 49, 48, 45, 42, 36, 34, and 33) and the GIS transect (Stns 55, 24, and 57), whereas expedition PS117consist of one transect – the Weddell Sea transect (Stns 95, 93, 91, 82, 85, 75, 73, 70, 67, 65, 61, and 56). The blue arrows in the Amundsen Sea indicate the path of modified Circumpolar Deep Water based on θ, S, and dissolved oxygen concentration (Tian et al., 2023b), where the blue arrows in the Weddell Sea indicate the edge of the Weddell Gyre.

relative to their commonly accepted zero standards for Zn (JMC-Lyon) and Cd (NIST-3108), respectively:

$$\delta^{66}Zn\,(\%) = \left\{ \left[\left({}^{66}Zn/{}^{64}Zn \right)_{sample} / \left({}^{66}Zn/{}^{64}Zn \right)_{JMC-Lyon} \right] - 1 \right\} \times 1000$$

and

$$\delta^{114}Cd\,(\%) = \left\{ \left[({}^{114}Cd/{}^{110}Cd)_{sample} / ({}^{114}Cd/{}^{110}Cd)_{NIST-3108} \right] - 1 \right\} \times 1000$$

However, since the supply of JMC-Lyon standard is limited, we use IRMM-3702 as a primary standard and convert $\delta^{66}Zn_{IRMM\text{-}3702}$ to $\delta^{66}Zn_{JMC\text{-}Lyon}$ by adding 0.29 ‰ to $\delta^{66}Zn_{IRMM\text{-}3702}$ (Archer et al., 2017; Moeller et al., 2012). As such, all $\delta^{66}Zn$ results reported in this study are relative to $\delta^{66}Zn_{JMC\text{-}Lyon}$.

Accuracy and external precision of MC-ICPMS analysis for $\delta^{66}Zn$ and $\delta^{114}Cd$ was assessed using the long-term delta value and precision of secondary isotope standards ($\delta^{66}Zn$: AA ETH, obtained from ETH Zürich; $\delta^{114}Cd$: BAM-I012, BAM Federal Institute for Materials Research and Testing).

Our long-term values (maen ± 2 SD) for AA ETH $\delta^{66}Zn$ and BAM-I012 $\delta^{114}Cd$ were + 0.27 ± 0.04 ‰ (n = 71 over 15 analytical sessions) and –1.33 ± 0.05 ‰ (n = 66 over 14 analytical sessions), respectively; both showed excellent agreement with literature values, demonstrating the accuracy of our analyses (see Supplementary Fig. S2). Consequently, we consider 0.04 ‰ and 0.05 ‰ to be conservative estimates of uncertainty for $\delta^{66}Zn$ and $\delta^{114}Cd$, respectively. We apply these values as standard deviation for all samples, except for those with 2 SE of an individual analysis larger than those values (13 % of all samples), in which case we use 2 SE as a measure of uncertainty (following Sieber et al., 2019a). For clarity, all isotope values reported in this study are means within 2 SD.

2.4. Auxiliary parameters, macronutrients, and oxygen isotope composition ($\delta^{18}O$)

2.4.1. Auxiliary parameters (salinity, temperature, depth) and fluorescence calibration

A calibrated CTD (Seabird SBE 911 +) with auxiliary sensors was mounted on the Titan sampling system to measure salinity (conductivity), temperature, depth (pressure), and fluorescence. The CTD-derived fluorescence was subsequently calibrated by measured total chlorophyll *a* concentration. Briefly, particulate samples for pigment-based phytoplankton taxonomic composition were collected through a GF/F glass fibre filter (45 mm diameter; Whatman, Cytiva, Marlborough, USA) at 1 °C, using a vacuum pump (200 mbar; Pal, Port Washington, NY, USA). Filters were double-wrapped in aluminium foil, snap-frozen in liquid nitrogen and stored at –80 °C until further analysis in the home lab. Further, pigments were dissolved in 90 % acetone (van Leeuwe et al., 2006), and measured on high-performance liquid chromatography (HPLC). The detailed procedure of this analysis and calibration is described in Eich et al. (2024) and Supplementary Fig. S3.

2.4.2. Macronutrients (PO_4 and $Si(OH)_4$)

Nutrient data for the ANA08B expedition were published by Tian et al. (2023b). For the PS117 expedition, unfiltered seawater samples (~50 mL) were collected for inorganic nutrient analysis, including PO_4 and silicic acid ($Si(OH)_4$). In the NIOZ shipboard analytical container, samples were transferred into 5 mL polyethylene vials (ponyvials) after rinsing three times with samples, capped, and stored at 4 °C. Prior to analysis, all samples and standards were brought to room temperature (~21–21.5 °C) within two hours in a dark drawer, then covered with parafilm to prevent evaporation. Nutrients were analysed on a Bran and Luebbe TRAAcs 800 Autoanalyzer within four to five hours of sampling. A detailed protocol is provided by Gerringa et al. (2019). Accuracy and precision for PO_4 and $Si(OH)_4$ were determined using a natural sterilized reference material (CA, Kanso, Japan, PO_4: 1.407 ± 0.014 μmol L^{-1}; $Si(OH)_4$: 36.58 ± 0.22 μmol L^{-1}) at 21.5 °C, resulting in values of 1.424 ± 0.008 μmol L^{-1} and 36.04 ± 0.17 μmol L^{-1}, respectively (n = 196).

2.4.3. Oxygen isotope composition ($\delta^{18}O$)

Oxygen isotope data for the ANA08B expedition were published by Tian et al. (2023b). For the PS117 expedition, dissolved seawater samples for $\delta^{18}O$ analysis were collected in 2 mL glass vials with polypropylene caps and inserts. $\delta^{18}O$ was measured using a Liquid Water Isotope Analyzer (LWIA, Los Gatos Research) at NIOZ, with an analytical precision of 0.16 ‰ (n = 13) based on duplicate measurements of an in-house standard (North Sea seawater-2018) over 13 sessions. The $\delta^{18}O$ values are reported relative to Vienna Standard Mean Ocean Water (VSMOW, International Atomic Energy Agency).

2.5. Phytoplankton pigment composition analysis

Samples were taken for pigment-based phytoplankton taxonomic composition analysis at one depth in the upper few tens of meters at selected stations in the Amundsen Sea (Stns 33, 34, 36, 42, 45, 49, 55, 24 and 57), whereas in the Weddell Sea, samples were taken at every station (also at one depth in the surface). The details of the taxonomic composition analysis are described in Eich et al. (2022) and Eich et al. (2024).

2.6. Production of figures

For the figures used in this study, Ocean Data View (ODV version 5.3.0, Schlitzer, 2020) was used to produce Figs. 1, 2, 6, 8, and S4. SigmaPlot (version 14.5) was used to produce Figs. 3, 4, 5, 7, S1, S2, S3, and S5. Fig. 9 was produced by Microsoft PowerPoint (Microsoft 365).

3. Results

3.1. Oceanographic setting

In the Amundsen Sea, three main water masses – mCDW, Winter Water (WW), and Antarctic Surface Water (AASW) – are identified by potential temperature (θ) and salinity (S) (Fig. 2a; Randall-Goodwin. et al., 2015). A detailed hydrography from the same expedition (ANA08B) has been reported in Tian et al. (2023b). In brief, intruding mCDW, located below 200–400 m at the open ocean station (Stn. 53) and the off-shelf station (Stn 55), has θ > 1°C and S > 34.5 (Fig. 2a, 2b, and 2c). As mCDW flows toward the Dotson Ice Shelf (DIS) (~200 m above the seafloor), its θ and S decrease to ~ –0.2 °C and 34.3 due to mixing with overlying waters before reaching the DIS (Fig. 2a). Beneath the DIS, outflowing mCDW (below 200 m at Stn 36, Tian et al., 2023b) further reduces to θ ~ –0.2 to –0.85 °C and S ~ 34.1 due to mixing with glacial meltwater (Fig. 2a). WW, formed by sea ice production and brine rejection, is situated between AASW and mCDW, with θ ~ –1.8 °C and S between 34 and 34.2 (Fig. 2a, 2b, and 2c). Near the surface along the DIS transect (Stns 50, 49, 48, 45, 34, and 33), AASW (~70 m depth) shows elevated θ (> 1.8 °C) and reduced S (< 34) due to sea ice melt and irradiation, whereas AASW along the Getz Ice Shelf (GIS) transect is located over a shallower depth interval (~25 m).

In the Weddell Sea, five water masses are identified: AASW (θ > –1.7 °C; S < 34.3), WW (θ minimum below AASW), Warm Deep Water (WDW, 0 > θ > 0.8 °C; 34.64 < S < 34.72), Weddell Sea Deep Water (WSDW, –0.7 °C < θ < 0°C; 34.64 < S < 34.68), and the precursor of Weddell Sea Bottom Water (pre-WSBW, θ < –0.7 °C at depth) (Fig. 2a; Fahrbach et al., 2004; Klatt et al., 2005). AASW occupies the upper ~ 70 m, and WW lies between ~ 70–250 m. In the eastern Weddell Sea, CDW enters via the Antarctic Circumpolar Current and mixes with AASW and WW to form WDW (230–1800 m) (Donnelly et al., 2017; Reeve et al., 2016). Mixing of WDW with uplifting WSBW generates WSDW at depths > 1500 m (Foster and Carmack, 1976). In the western Weddell Sea,

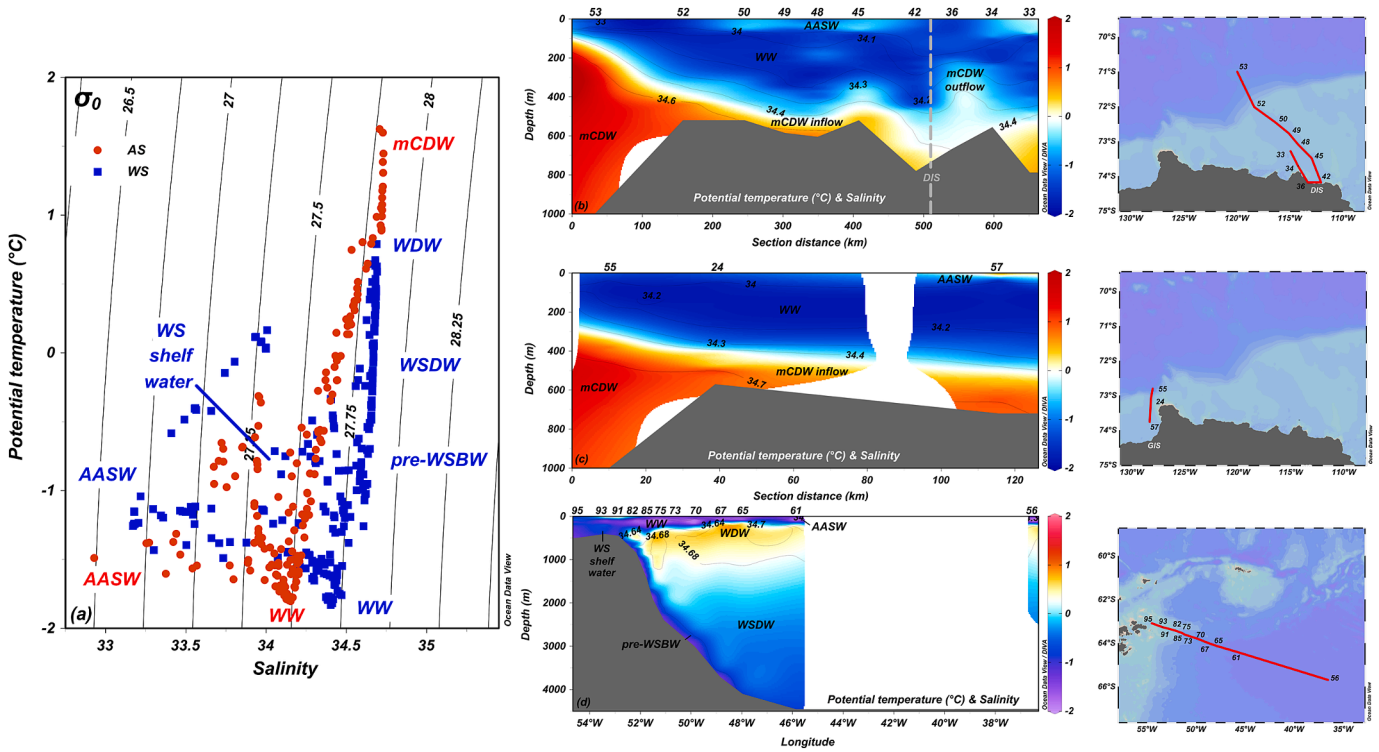

Fig. 2. (a) Potential temperature (θ)-salinity (S) diagram of all ANA08B (the Amundsen Sea) and PS117 (the Weddell Sea) stations. Section profiles of θ and S of (b) the Dotson Ice Shelf (DIS) transect, (c) the Getz Ice Shelf (GIS) transect, and (d) the Weddell Sea transect. The color grading and density isocline in (b) to (d) represent θ and S, respectively.

dense shelf water forms in winter through cooling and brine rejection on the Antarctic continental shelf (i.e., the shelf stations). During summer (sampling period of GApr12-PS117), stratification occurs with warmer AASW near the surface (Fig. 2a and 2d). For clarity, in this study, the term 'dense shelf water' refers to the dense and cold water formed only in winter, whereas the term 'WS shelf water' refers to the shelf water observed at the shelf stations (deeper than AASW) in this study. Subsequently, dense shelf water descends and interacts with WDW and WSDW along the slope and eventually forms WSBW (Foster and Carmack, 1976; Vernet et al., 2019). Here, we characterise this descending water mass (also observed in summer) as the precursor of WSBW (pre-WSBW, θ < –0.7 °C, 150–200 m above the continental slope sediments, Fig. 2a and 2d). Ultimately, the mixture of pre-WSBW, WDW, and WSDW leaves the Weddell Sea at north-western site, as a key source of AABW (Orsi et al., 1999). It should be noted that WSBW is usually situated deeper than ~ 3500 m in this region (e.g., Gordon et al., 2001), which is not observed in this study since most stations were located closer to the Antarctic Peninsula with shallower bottom depths (Fig. 2d).

3.2. Weighted average of chlorophyll a concentration ([chl a]$_{wt.avg}$)

In the Amundsen Sea, chlorophyll *a* concentration ([chl *a*]) increases from the surface to ~ 70 m, while in the Weddell Sea, it peaks at ~ 90 m. This depth range, from the surface to the [chl *a*] maximum, is defined as the surface layer. To assess productivity within this layer, we calculated the weighted average of [chl *a*] ([chl *a*]$_{wt.avg}$) by integrating the concentration over depth and dividing by the surface layer depth (Supplementary Fig. S3). The [chl *a*]$_{wt.avg}$ is notably higher in the Amundsen Sea (3.48 ± 2.89 μg L^{-1}) than in the Weddell Sea (0.13 ± 0.09 μg L^{-1}). In the Amundsen Sea, most stations exhibit [chl *a*]$_{wt.avg}$ > 2 μg L^{-1}, except for Stns 53 and 52. Stations with [chl a]$_{wt.avg}$ > 2 μg L^{-1} are categorized as bloom stations, specifically DIS bloom stations (Stns 50, 49, 48, 45, 42, 36, 34, 33) and GIS bloom stations (Stns 55, 24, 57). Conversely, stations in the Weddell Sea, where [chl *a*]$_{wt.avg}$ remains consistently low, are not considered bloom stations and referred to as WS stations (Supplementary Fig. S3).

3.3. Phytoplankton community composition

In the Amundsen Sea, haptophytes dominated the phytoplankton community along the DIS transect, contributing 59 % to nearly 100 %, with the highest proportions at Stns 45 (99.9 %) and 49 (99.4 %). In contrast, diatoms dominated the GIS transect, comprising 54–91 %, especially at Stns 55 (91.3 %) and 24 (87.9 %) (Eich et al., 2024; Tian et al., 2023b, Supplementary Fig. S3). Along the Weddell Sea transect, no single group dominated; other species such as dinoflagellates, cryptophytes, chlorophytes, and pelagophytes contributed significantly, accounting for ~ 21 % to ~ 59 % (Supplementary Fig. S3).

3.4. Freshwater input ($\delta^{18}O$)

This study uses $\delta^{18}O$ to estimate freshwater input, including sea-ice melt and meteoric water (e.g., ice sheet or iceberg meltwater). Previously, the fraction of sea-ice melt and meteoric water were estimated for the Amundsen Sea (Tian et al., 2023b), using a three-component mass balance model described in Randall-Goodwin. et al. (2015). Since the Weddell Sea shelf stations are located near the Antarctic Peninsula where large ice shelves are situated (e.g., Larsen Ice shelf, Nicholls et al., 2009), meltwater from the ice shelf may have biogeochemical impacts on these shelf stations. Here, we modified the mass balance model used in Tian et al. (2023b) for the Weddell Sea (modifications of the model and endmembers are detailed in Supplementary Fig. S3). Based on the mass balance model, the estimated fraction of meteoric water (f_{met}) in the upper 250 m at the shelf stations ranges from 0.3 % to 4.8 %, where the highest f_{met} estimate is found close to the shore (i.e., Stn 95) with lower values towards offshore (i.e., Stn 91) (Supplementary Fig. S4).

3.5. Dissolved Zn and Cd concentrations and their isotope compositions

3.5.1. The Amundsen Sea

The dissolved Zn and Cd concentrations ([dZn] and [dCd]) for the Amundsen Sea (ANA08B expedition) were previously described in-depth by Tian et al. (2023b). As such, we just provide a simple overview here and focus on the isotope ratios. In the Amundsen Sea, [dZn] and [dCd] ranged from 0.87 to 7.67 nmol L^{-1} and from 0.05 to 0.87 nmol L^{-1}, respectively (Fig. 3). Lower concentrations were observed in the surface layer of bloom stations, whereas higher values were found at non-bloom stations (Stns 53 and 52, Fig. 3). Furthermore, surface [dZn] and [dCd] were lower at GIS bloom stations (0.87–5.47 and

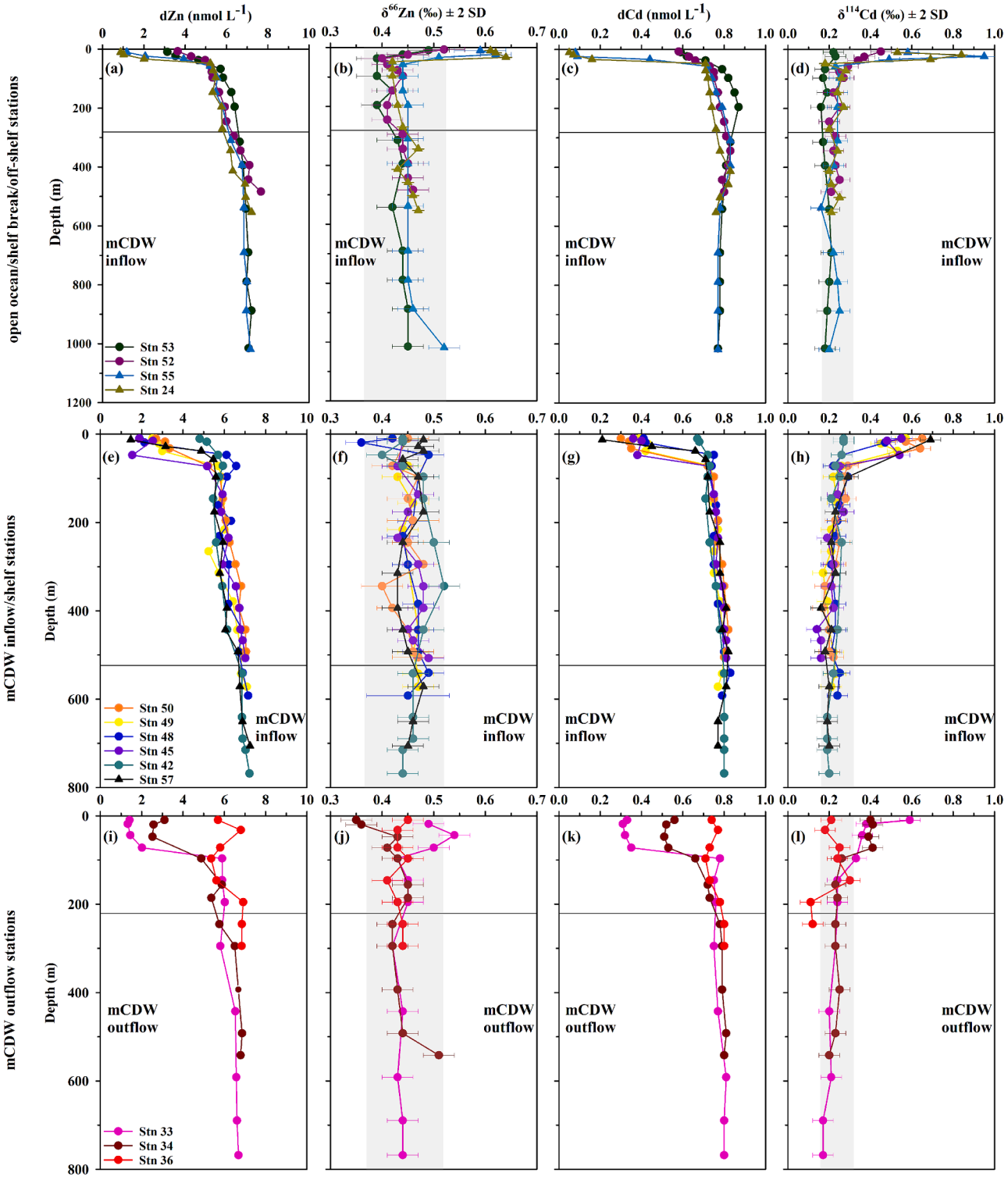

Fig. 3. Dissolved elemental concentrations ([dZn] and [dCd]) and isotope compositions (δ^{66}Zn and δ^{114}Cd) of all Amundsen Sea (ANA08B) stations. (a) to (d) the open ocean/shelf break/off-shelf stations; (e) to (h) the mCDW inflow stations; (i) to (l) the mCDW outflow stations. The grey shadings indicate the deep-water signature of δ^{66}Zn (+0.44 ± 0.08 ‰, Bermin et al., 2006; Conway and John, 2014; Lemaitre et al., 2020; Sieber et al., 2020) and of δ^{114}Cd (+0.25 ± 0.06 ‰, Abouchami et al., 2014; Conway and John, 2015; George et al., 2019; Xie et al., 2017). The error bars for δ^{66}Zn and δ^{114}Cd are two standard deviations.

0.05–0.71 nmol L^{-1}, respectively) compared to DIS bloom stations (1.33–6.80 and 0.30–0.77 nmol L^{-1}, respectively, Fig. 3). Both [dZn] and [dCd] generally increased with depth, reaching > 7 nmol L^{-1} and > 0.8 nmol L^{-1} near the seafloor on the continental shelf (where mCDW inflow situated) and in deep open-ocean waters (where the least modified CDW is found, identified by higher θ, Fig. 3).

Dissolved Zn and Cd isotope compositions (δ^{66}Zn and δ^{114}Cd) in the Amundsen Sea ranged from + 0.35 to + 0.64 ‰ and + 0.11 to + 0.95 ‰, respectively (Fig. 3). The heaviest isotope signatures in these ranges for both elements were observed in the surface layer of GIS bloom stations (δ^{66}Zn: up to + 0.64 ‰; δ^{114}Cd: up + 0.95 ‰), whereas at DIS bloom stations the signatures were lighter (δ^{66}Zn: up to + 0.44 ‰; δ^{114}Cd: up to + 0.65 ‰) (Fig. 3). Most δ^{114}Cd values decreased with increasing depth and became relatively constant (+0.21 ± 0.07 ‰) below ~ 100 m, whereas for δ^{66}Zn the decreasing trend (from the surface to ~ 100 m) was only apparent at GIS bloom stations, the open ocean/shelf break/off-shelf stations, and two of the mCDW outflow stations (i.e., Stns 34 and 33); whereas the other stations were characterised by relatively homogeneous δ^{66}Zn from the surface to the deep ocean (+0.45 ± 0.05 ‰, Fig. 3).

3.5.2. The Weddell Sea

In the Weddell Sea, [dZn] and [dCd] ranged from 3.56 to 8.57 nmol L^{-1} and from 0.56 to 0.64 nmol L^{-1}, respectively (Fig. 4). δ^{66}Zn and δ^{114}Cd ranged from + 0.34 to + 0.50 ‰ and + 0.07 to + 0.44 ‰, respectively; smaller ranges than observed in the Amundsen Sea (Fig. 4). The lowest [dZn] and [dCd] coincided with the highest isotope ratios and were typically observed in the upper 50 m of the surface layer. Generally, [dZn] and [dCd] increased (and isotope ratios decreased) with increasing depth below the surface layer.

At the shelf stations (Stns 91, 93 and 95), [dZn] and [dCd] reached maximum values below 100–150 m (5.63 ± 0.39 nmol L^{-1} and 0.76 ± 0.02 nmol L^{-1}, respectively) at Stn 93 and 91, whereas Stn 95 exhibited relatively constant (and lower than Stns 91 and 93) [dZn] (4.58 ± 0.29 nmol L^{-1}) and [dCd] (0.69 ± 0.02 nmol L^{-1}) throughout the water column (Fig. 4). At all three shelf stations, δ^{66}Zn was relatively homogeneous throughout the water column (+0.42 ± 0.04 ‰), whereas δ^{114}Cd decreased from ~+0.41 ‰ at the surface to ~+0.20 to + 0.30 ‰ at ~ 100 m and became homogeneous below 100 m (+0.27 ± 0.04 ‰) (Fig. 4).

At the continental slope stations (Stns 82, 85, 75, 73, 70, and 67), both [dZn] and [dCd] increased with depth until 100–150 m above the sediments of the continental slope where descending pre-WSBW was located with lower [dZn] (5.73 ± 0.39 nmol L^{-1}) and [dCd] (0.75 ± 0.01 nmol L^{-1}, Fig. 4). δ^{66}Zn were generally homogeneous throughout the water column (+0.41 ± 0.05 ‰, Fig. 4). In contrast, δ^{114}Cd reached ~+0.40 ‰ in the surface layer of several continental slope stations (i.e., Stns 82, 85, 75, and 73), whereas at the other two stations (Stns 70 and 67) δ^{114}Cd were lower in surface waters (+0.23 ± 0.09 ‰). The elevated surface δ^{114}Cd values decreased with increasing depth. Below 500 m, δ^{114}Cd at all continental slope stations was homogeneous (+0.24 ± 0.05 ‰, Fig. 4).

At the offshore stations (Stns 65, 61, and 56), [dZn] and [dCd] increased with depth (as high as 8.34 nmol L^{-1} and 0.94 nmol L^{-1}, respectively). Below ~ 1000 m, both [dZn] and [dCd] decreased with depth to ~ 7.10 nmol L^{-1} and 0.80 nmol L^{-1}, respectively, where WSDW was situated (Fig. 4). At these stations, δ^{66}Zn was homogeneous (within the range of global deep-water signal) throughout the water column. In contrast, δ^{114}Cd values up to ~+0.32 ‰ were observed in the surface and gradually decreased with depth, reaching a minimum of + 0.07 ‰ between ~ 250 m and ~ 1500 m at Stns 61 and 56, whereas Stn 65 exhibits homogeneous δ^{114}Cd below ~ 250 m (+0.23 ± 0.04 ‰) (Fig. 4).

4. Discussion

4.1. δ^{66}Zn and δ^{114}Cd signatures of previously identified potential external sources

The isotope compositions of the least modified CDW (Stn 53 δ^{66}Zn: +0.44 ± 0.03 ‰; δ^{114}Cd: +0.20 ± 0.03 ‰, Fig. 3b and 3d) align with the global deep-water signals for δ^{66}Zn (+0.44 ± 0.08 ‰, e.g., Bermin et al., 2006; Conway and John, 2014; Lemaitre et al., 2020; Sieber et al., 2020; Sieber et al., 2023; Takano et al., 2017) and δ^{114}Cd (+0.25 ± 0.06 ‰, e.g., Abouchami et al., 2014; Conway and John, 2015; George et al., 2019; Sieber et al., 2023b; Xie et al., 2017; Xie et al., 2019; Yang et al., 2012). These signatures remain consistent (overlapping within uncertainty) over the continental shelf, including shelf break stations, mCDW inflow stations, and shelf stations, within 200 m above the seafloor (δ^{66}Zn: +0.46 ± 0.04 ‰; δ^{114}Cd: +0.21 ± 0.06 ‰, Fig. 3f and 3 h).

To date, there are no reported isotope signatures for Zn and Cd in AS shelf sediments, whereas global marginal sediments and lithogenic sources show lower values (δ^{66}Zn: –0.72 to + 0.32 ‰, Conway and John, 2014; Lemaitre et al., 2020; Little et al., 2016; δ^{114}Cd: –0.01 ± 0.04 ‰, Bryan et al., 2021; Chen et al., 2021; Rehkämper et al., 2012; Schmitt et al., 2009) compared to deep waters. Based on these reported ranges, the isotope change between observed signatures and sediment signatures are –1.18 to –0.14 ‰ and –0.25 to –0.18 ‰, for δ^{66}Zn and δ^{114}Cd, respectively, on the AS continental shelf. Further, applying estimated contributions of sedimentary Zn (7 %) and Cd (4 %) from AS shelf sediments to the overlying waters reported by Tian et al. (2023b), we estimate a change in isotope signature for δ^{66}Zn (–0.08 to –0.01 ‰) and for δ^{114}Cd (–0.010 to –0.007 ‰) on observed signatures, assuming the shelf sediment is a secondary source (in addition to mCDW) of both elements. Despite the variability in reported sedimentary signatures, these small additions fall within the uncertainty of deep-water signals. Consequently, the consistent isotope signatures in mCDW inflow suggest that the external sedimentary input is similar to the deep-water signals or, more likely, the magnitude of sedimentary addition is too small to alter mCDW isotope signatures.

There is no statistically significant difference in δ^{66}Zn and δ^{114}Cd between the mCDW inflow, outflow, and shelf water adjacent to the DIS (Table 1), implying that the DIS may be a negligible source of Zn and Cd, as suggested by Tian et al. (2023b). However, constraints on glacial δ^{66}Zn remain limited. Sieber et al. (2020) speculated that glacial meltwater could supply Zn with an isotope signature close to the continental crust (+0.3 ‰, Little et al., 2014) to surface waters near the Mertz Glacier (East Antarctica). For Cd, there is no information on δ^{114}Cd from glaciers. Therefore, it is possible that glacial δ^{66}Zn and δ^{114}Cd are similar to mCDW, making it indistinguishable by isotope signatures. This speculation requires further constraints on the endmembers of Antarctic glacial isotope compositions.

Overall, the isotope data show that mCDW is the primary source of dZn and dCd to the AS, with minor contributions from shelf sediments and the DIS, consistent with previous studies based on concentration data (Sherrell et al., 2015; Tian et al., 2023b).

4.2. Isotope signatures of Zn and Cd in the Weddell Sea

In contrast to the Amundsen Sea, where mCDW intrusion is critical for trace element biogeochemistry, the Weddell Sea is influenced by gyre circulation and pre-WSBW formation, which eventually flows northward into global ocean basins (e.g., Vernet et al., 2019). Consequently, trace element biogeochemistry in the Weddell Sea may impact regional and global cycling through the export of Weddell Sea waters. In the following section, we 1) evaluate glacial meltwater contributions of dZn and dCd to the Weddell Sea, 2) discuss the lack of isotope signature changes during deep water formation, and 3) speculate on differences in isotope signatures between the outer and inner Weddell Gyre.

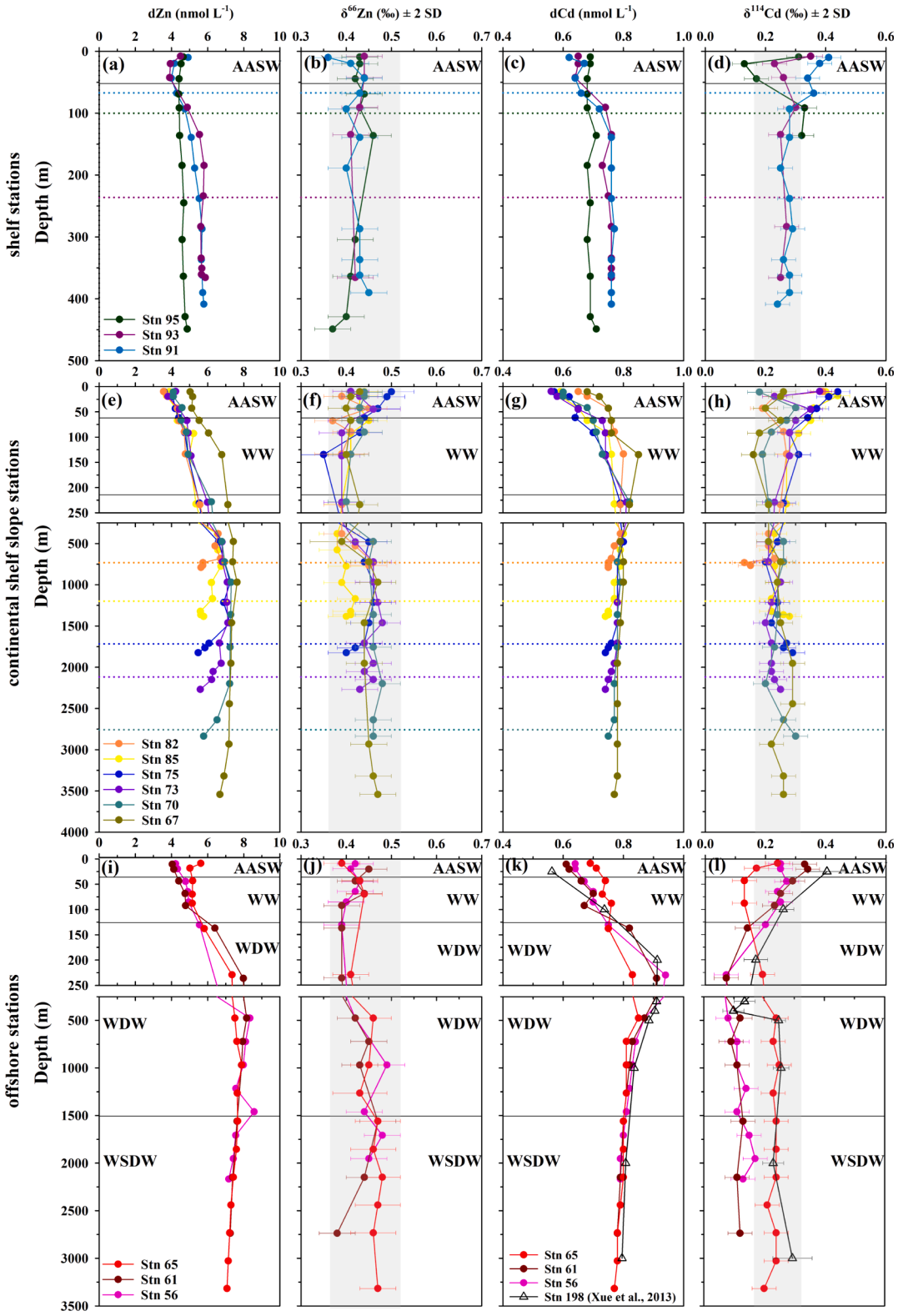

Fig. 4. Dissolved elemental concentrations ([dZn] and [dCd]) and isotope compositions (δ^{66}Zn and δ^{114}Cd) of all Weddell Sea (PS117) stations. (a) to (d) the shelf stations; (e) to (h) the continental slope stations; (i) to (l) the off-shore stations. The grey shadings indicate the deep-water signature of δ^{66}Zn (+0.44 ± 0.08 ‰) and of δ^{114}Cd (+0.25 ± 0.06 ‰). The colored dotted lines in (a) and (d) indicate the upper bound of WS shelf water defined based on a neutral density of < 28.0 kg m^3 and $\theta < -0.7$ °C at the shelf stations, whereas the colored dotted lines in (e) and (h) indicate the upper bound of pre-WSBW defined based on $\theta < 0.7$ °C. In (k) and (l), the open symbols represent the data obtained from a station previously reported by Xue et al. (2013), which was close to the offshore stations in this study. The error bars for δ^{66}Zn and δ^{114}Cd are two standard deviations.

Table 1
$\delta^{66}Zn$ and $\delta^{114}Cd$ in the mCDW outflow, the mCDW outflow, and Amundsen Sea shelf water along the DIS transect. For the mCDW inflow, following the path of the inflow (Fig. 5b), $\delta^{66}Zn$ and $\delta^{114}Cd$ within 100 m above the seafloor at st. 45 were selected (Tian et al., 2023; Tian et al., 2023b) as Stn 45 is expected to represent the mCDW inflow better than Stn 42 that is closer to the DIS due to potential lithogenic material input at Stn 42 (van Manen et al., 2022). For the mCDW outflow, $\delta^{66}Zn$ and $\delta^{114}Cd$ between 195 to 295 m at Stn 36 were selected, based on θ (> –1℃) and salinity (> 34.1). The outflow was located at a similar depth as previously reported for the core of mCDW outflow (200 to 400 m, Miles et al., 2016; Randall-Goodwin. et al., 2015). For the Amundsen Sea shelf water, to represent the ambient waters located around the DIS, $\delta^{66}Zn$ and $\delta^{114}Cd$ were selected from the closest station (i.e., Stn 42) to the DIS within the depth (145 to 300 m) of mCDW outflow (Tian et al., 2023b).

	station	depth (m)	$\delta^{66}Zn \pm 2$ SD (‰)	$\delta^{114}Cd \pm 2$ SD (‰)
mCDW inflow	45	442	+0.45 ± 0.03	+0.14 ± 0.05
		467	+0.46 ± 0.03	+0.16 ± 0.05
		507	+0.49 ± 0.03	+0.16 ± 0.05
		mean ± 2 SD	+0.47 ± 0.04	+0.15 ± 0.02
Amundsen Sea shelf water	42	145	+0.48 ± 0.03	+0.21 ± 0.05
		245	+0.50 ± 0.03	+0.26 ± 0.05
		344	+0.52 ± 0.03	n/a
		mean ± 2 SD	+0.50 ± 0.05	+0.20 ± 0.08
mCDW outflow	36	195	+0.43 ± 0.03	+0.11 ± 0.05
		245	+0.44 ± 0.03	+0.12 ± 0.05
		294	+0.44 ± 0.03	n/a
		mean ± 2 SD	+0.44 ± 0.01	+0.11 ± 0.01

4.2.1. The shelf station (Stn 95): modest glacial meltwater influence

At the shelf stations, meteoric water input (f_{met}) is elevated at Stn 95 (up to 4.8 %, shallower than ~ 250 m) and decreases towards the central Weddell Sea basin (Supplementary Fig. S4). The maximum meltwater fractions in the Weddell Sea are much higher than the maximum f_{met} (~0.64 %) for the mCDW outflow in the Amundsen Sea (Tian et al., 2023b). The increasing f_{met} towards the Antarctic Peninsula allows us to evaluate glacial meltwater influence on [dZn], [dCd], and their isotope compositions in the Weddell Sea.

Since any glacier-derived dZn and dCd in the surface layer (approximately the upper 90 m, section 3.2) may be modulated by biological activity such as uptake, it is more sensible to assess samples below the surface layer (i.e., 90 to 250 m), in order to evaluate meltwater influence. Within this depth range, Stn 95 showed consistently lower [dZn] (4.65 ± 0.27 nmol L^{-1}) and [dCd] (0.69 ± 0.03 nmol L^{-1}) compared to the other two shelf stations with lower meltwater contributions ([dZn]: 5.51 ± 0.66 nmol L^{-1}; [dCd]: 0.76 ± 0.02 nmol L^{-1}) (Fig. 4a and 4c). This suggests that meltwater at Stn 95 contains less Zn and Cd, effectively diluting [dZn] and [dCd]. Further, it seems that conservative mixing of meltwater (lowest [dZn] and [dCd]) and shelf waters (low [dZn] and [dCd]) with offshore waters (high [dZn] and [dCd], e.g., WDW) accounts for the observed variability in concentrations between shelf stations (Fig. 4). The strong linear relationship ($p < 0.001$) between S and dissolved concentrations in Weddell Sea shelf waters and WDW further supports conservative mixing (Fig. 5a and 5d), explaining the increase in concentrations at the other shelf stations compared to Stn 95 (Fig. 4e and 4f). Despite differences in [dZn] and [dCd] between Stn 95 and the other shelf stations, $\delta^{66}Zn$ (+0.42 ± 0.03 ‰) and $\delta^{114}Cd$ (+0.28 ± 0.06 ‰) were similar to deep-water values at all three shelf stations in the 90–250 m range (Fig. 4b and 4d). This indicates that glacial meltwater either does not supply sufficient Zn and Cd to alter the isotope signature, or has isotope compositions similar to mCDW, making it indistinguishable in the observed isotope data. This finding is consistent with observations in the Amundsen Sea (section 4.1).

4.2.2. The continental slope stations: consistent $\delta^{66}Zn$ and $\delta^{114}Cd$ in shelf and deep waters

Since the Weddell Sea exports a major component of northwards-advecting AABW (formed from WSDW and WSBW) into the global ocean (e.g., Huhn et al., 2008; Orsi et al., 1999; Vernet et al., 2019), one of the objectives of this study is to investigate changes in [dZn], [dCd], $\delta^{66}Zn$, and $\delta^{114}Cd$ during deep water formation. Pre-WSBW is characterised by indistinguishable [dZn] and [dCd] to WS shelf water, while WDW and WSDW have significantly higher [dZn] and [dCd] (Fig. 4a and 4c). The linear relationship between S and dissolved concentrations in WS shelf water, pre-WSBW, WDW (Stns 82 to 67), and WSDW (Stns 75 to 67) suggests that physical mixing drives the increase in concentrations during the descendent of pre-WSBW along the slope (Fig. 5a and 5d). However, a few shallower samples (90–190 m) with high [dCd] (0.72–0.76 nmol L^{-1}) and lower S (34.43–34.53) deviate from this trend, possibly due to shallow remineralization, as indicated by elevated PO_4 (Fig. 5d and 5e).

In contrast to [dZn] and [dCd], $\delta^{66}Zn$ and $\delta^{114}Cd$ are homogeneous across WS shelf water, pre-WSBW, WDW, and WSDW, showing no relationship with S (Fig. 5c and 5f). The consistent $\delta^{66}Zn$ and $\delta^{114}Cd$ signatures from the continental shelf to the slope suggest minimal sediment input along the slope, as such inputs would lead to lighter isotope signatures (e.g., Conway and John, 2014; Lemaitre et al., 2020; Liao et al., 2020; Little et al., 2016; Rehkämper et al., 2012; Schmitt et al., 2009). This observation in the Weddell Sea aligns with findings from the Amundsen Sea, indicating a modest supply of Zn and Cd from sediments (section 4.1).

Comparison of $\delta^{66}Zn$ and $\delta^{114}Cd$ in these water masses with those previously reported for WSBW and WSDW in the Weddell Sea (Abouchami et al., 2014; Xue et al., 2013; Zhao et al., 2014) and AABW further north in the global basin (Conway and John, 2014, 2015; John et al., 2018), reveals nearly identical $\delta^{66}Zn$ and $\delta^{114}Cd$ across different deep-water masses (Fig. 5c and 5f). This suggests that homogeneous Zn and Cd isotope compositions in global deep waters are already established in forming AABW (i.e., dense shelf water and pre-WSBW). A similar 'preformed' $\delta^{114}Cd$ signal in subsurface waters (~100 m) has also been reported by Janssen et al. (2017) and Sieber et al. (2019a), with physical mixing identified as the main driver of deep-water $\delta^{114}Cd$ (Guinoiseau et al., 2019). This observation further aligns with previous findings that ventilated deep water can retain the signals of dissolved macro/micronutrients (e.g., Middag et al., 2013) and $\delta^{114}Cd$ (e.g., Xue et al., 2013) in the surface and transport these signals into the deep Weddell Sea basin.

While isotope compositions remain uniform in Weddell Sea deep waters, dissolved concentrations may increase as Weddell Sea deep waters flow into the deep global ocean. For example, the deep Pacific Ocean exhibits similar and uniform $\delta^{66}Zn$ and $\delta^{114}Cd$, with slightly higher [dZn] (~1 nmol L^{-1} higher; Sieber et al., 2023) and [dCd] (~0.1 nmol L^{-1} higher; Sieber et al., 2023b), than Weddell Sea deep waters. This uniformity in isotopic signatures is likely because Southern Ocean-sourced deep waters already carry abundant Zn and Cd, effectively overprinting any (subtle) variations in isotope compositions caused by remineralization or mixing (Janssen et al., 2017; Sieber et al., 2019a). Consequently, the observed increase in metal concentrations in the Pacific occurs without altering the isotope compositions, highlighting the pivotal role of the Southern Ocean and the Weddell Sea in regulating the Cd distribution in deep waters (Janssen et al., 2017; Sieber et al., 2023b), and most probably the Zn distribution as well (Sieber et al., 2023).

4.2.3. The offshore stations: enhanced remineralization signal in the inner Weddell Gyre

At the offshore stations, akin to the continental slope stations, $\delta^{66}Zn$ remains uniform (i.e., deep-water isotope composition) throughout the water column (Fig. 4j). By contrast, a striking feature is observed for $\delta^{114}Cd$ at both offshore Stns 61 and 56 (close to the central Weddell Sea,

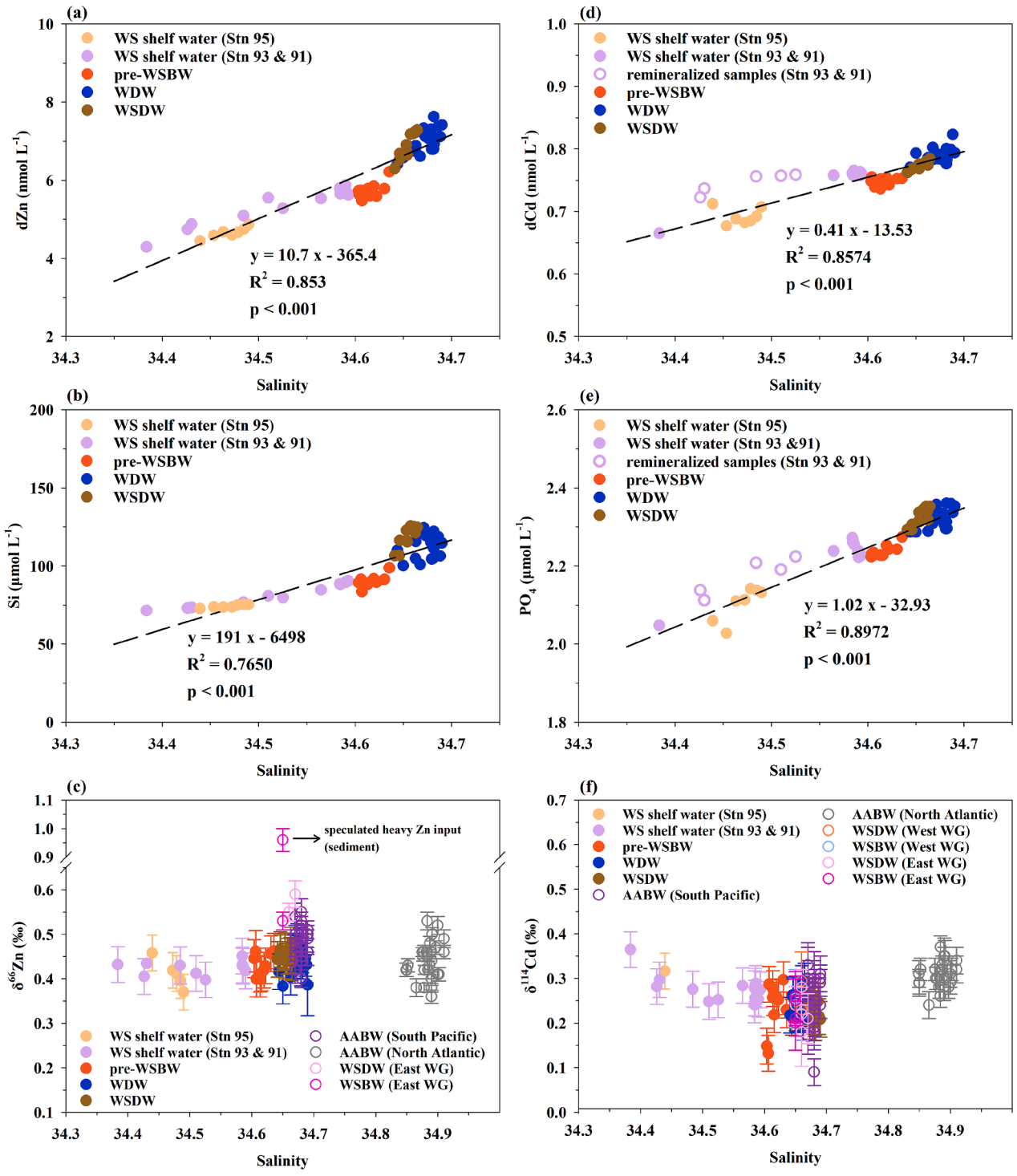

Fig. 5. Correlations of salinity with (a) [dZn]; (b) [Si]; (c) δ^{66}Zn; (d) [dCd]; (e) [PO_4]; (f) δ^{114}Cd in different water masses observed along the Weddell Sea transect (dense shelf water, pre-WSBW, WDW, and WSDW). For (d) and (e), the open symbols indicate the samples with shallow remineralization signals; the correlation does not include these samples. For (c), open symbols represent the previously reported δ^{66}Zn values (±2 SD) in AABW (South Pacific: John et al., 2018; North Atlantic: Conway and John, 2015), WSDW and WSBW (East Weddell Gyre: Zhao et al., 2014). For (f), the open symbols represent the previously reported δ^{114}Cd values (±2 SD) in AABW (South Pacific: John et al., 2018; North Atlantic: Conway and John, 2015), WSDW and WSBW(East Weddell Gyre: Xue et al., 2013; West Weddell Gyre: Abouchami et al., 2014).

referred to the inner gyre stations in this section) where δ^{114}Cd is noticeably lower (as low as + 0.07 ‰) between ~ 250 m and ~ 1500 m and gradually increases towards (but not fully, ~+0.17 ‰) the global deep-water signal below 1500 m, whereas at Stn 65 (close to the peninsula, referred to the outer gyre station) δ^{114}Cd is homogeneous below ~ 250 m (+0.23 ± 0.04 ‰, within the uncertainty of global deep-water signature) (Fig. 4l).

Previously at a nearby location, Xue et al. (2013) observed a similarly low δ^{114}Cd signal (~+0.10 ‰) between 200 m and 400 m at a Weddell Sea station (station 198, ~65°S, ~36°W) for samples collected 11 years prior. However, δ^{114}Cd abruptly returned to global deep-water signature below 400 m (Fig. 4l). Using a mass balance model, they

concluded that such low δ^{114}Cd results from remineralization of biomass with isotopically light Cd produced in the surface, which aligns with our observation of a [dCd] maximum at ~ 250 m, coinciding with the lowest δ^{114}Cd. However, this theory only explains the isotopically light signature between 200 m and 400 m. The continuation of the light δ^{114}Cd from 400 m to ~ 1500 m may be due to slow ventilation in the inner gyre stations (Stns 61 and 56) compared to the outer gyre station (Stn 65) (Fig. 1). First, apparent oxygen utilization (AOU) is higher between 250 m and 1500 m in the inner gyre station (Stn 61; AOU data for Stn 56 are unavailable due to a malfunctioning oxygen sensor) than in the outer gyre station (Fig. 6a), indicating older water and stronger overall remineralization at the former station. Furthermore, the highest θ (> 0.75 °C) is observed between 200 m and 400 m near the outer gyre (Stn 65, 64°S, 48°W), while relatively low θ (< 0.75 °C) are found in the inner gyre (Stns 61 and 56) at similar depths (Fig. 6b). This gradient is attributed to the western boundary current of the Weddell Gyre (e.g., Fahrbach et al., 1994), which likely separates Stns 61 and 56 from the other WS stations. The location of the western boundary between Stns 65 and 61 agrees with Argo float data showing the north-eastward limb of the Weddell Gyre between ~ 63-65°S and ~ 40-50°W (Reeve et al., 2016). We propose that slow ventilation in the central gyre results in relatively isolated water that accumulates remineralization products down to ~ 1500 m, leading to an isotopically light Cd signature. In contrast, waters at the gyre edge are more affected by lateral circulation of WDW. As such, the differences in δ^{114}Cd between Stns 61, 56, and 65 likely indicate distinct biogeochemical features between the inner and outer Weddell Gyre.

Conversely, δ^{66}Zn shows no significant difference between the inner and outer gyre (Fig. 4j). We postulate that this may be due to weaker and less distinct isotope fractionation during surface uptake (section 4.3.2), resulting in a less pronounced remineralization signal inside the gyre. A more complex interaction of surface processes may influence δ^{66}Zn in particulate materials (e.g., diatom frustules, organic tissues, or adsorbed phases), with different Zn phases regenerating at depth, leading to a less distinct remineralization signal. However, δ^{66}Zn data in the Weddell Gyre are scarce, with only Zhao et al. (2014) in the east Weddell Gyre and this study in the west Weddell Gyre, compared to δ^{114}Cd data. We note that this speculation requires further investigation, including particulate Zn isotope compositions, to determine if speciation (e.g., Köbberich and Vance, 2018), scavenging (e.g., John and Conway, 2014; Sieber et al., 2023b; Weber et al., 2018) or remineralization (e.g., Samanta et al., 2017; Sieber et al., 2020) drives δ^{66}Zn in both the inner and outer Weddell Gyre.

4.3. Variability in isotope signatures in the surface water of the Amundsen Sea and the Weddell Sea

Biological assimilation plays a key role in regulating dissolved Zn and Cd in coastal Antarctic surface waters, such as the Amundsen Sea and the Weddell Sea (Abouchami et al., 2014; Janssen et al., 2020; Sherrell et al., 2015; Sieber et al., 2019a; Tian et al., 2023b; Zhao et al., 2014). Biological uptake causes isotope fractionation in seawater for both elements (Conway and John, 2014; Köbberich and Vance, 2019; Lacan et al., 2006; Ripperger et al., 2007; Samanta et al., 2018; Sieber et al., 2019a), making δ^{66}Zn and δ^{114}Cd in the Amundsen Sea and the Weddell Sea useful for investigating Zn and Cd uptake by phytoplankton, as well as the mechanisms controlling their isotope systematics. In this section, we focus on data in the surface layer (i.e., between the surface and [chl *a*] maximum depth) for both the Amundsen Sea bloom stations – except for Stns 36 and 42 as elevated surface [dZn] and [dCd] suggests terrestrial input that may hinder the investigation of biological uptake processes (Fig. 3) – and the WS stations.

4.3.1. δ^{114}Cd systematics in the surface layer: biological uptake predominantly drives δ^{114}Cd

Biological uptake dominates surface δ^{114}Cd signatures in both the

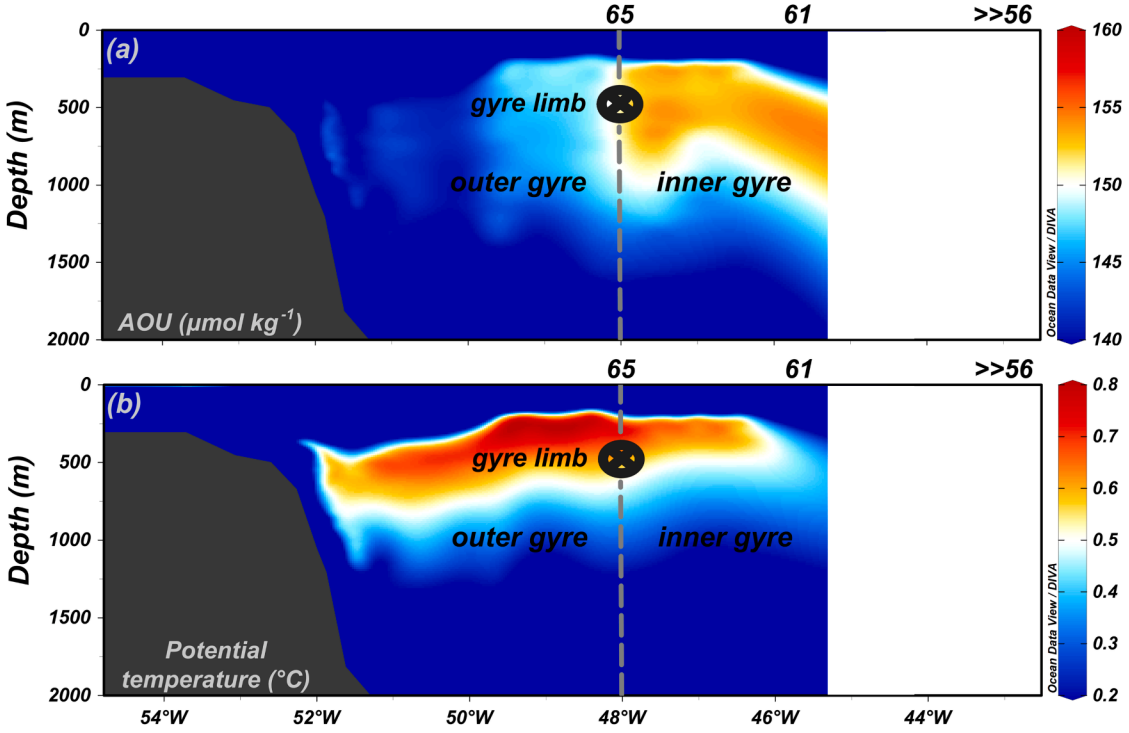

Fig. 6. (a) Apparent oxygen utilization (AOU) and (b) potential temperature (θ) at the offshore stations along the Weddell Sea transect. AOU is converted by Ocean Data View (ODV version 5.3.0, Schlitzer, 2020), using dissolved oxygen data obtained from oxygen sensor installed on the regular CTD deployed by the research team of Alfred Wegener Institute for Polar and Marine Research, at stations close to the trace element stations (where the Titan CTD system without functioning oxygen sensor was used). The dashed lines indicate Stns 65 and 61 (AOU at Stn 56 is not available). The location of the gyre limb is determined based on the observation of Reeve et al., (2019) and the section profiles of AOU and θ. The black cross and circle indicate the direction (pointing into the screen) of the Weddell Gyre.

Amundsen Sea and the Weddell Sea, with δ^{114}Cd up to + 0.95 ‰ in the Amundsen Sea bloom stations and up to + 0.44 ‰ in the Weddell Sea, compared to a deep ocean value of ~+0.25 ‰. The lowest [dCd] generally correspond to higher δ^{114}Cd, indicating preferential uptake of light Cd isotopes in the surface (Fig. 7d, 7e, and 7f) (e.g., Abouchami et al., 2011; Conway and John, 2014; Lacan et al., 2006; Ripperger et al., 2007; Sieber et al., 2019). An inverse relationship between [dCd] and δ^{114}Cd follows Rayleigh fractionation trends (closed system), with fractionation factors (α, where $\alpha = R_{biomass}/R_{seawater}$) ranging from 0.99930 to 0.99995 in the Amundsen Sea and 0.99800 to 0.99900 in the Weddell Sea (Fig. 7d, 7e, and 7f), in agreement with previous Southern Ocean observations (0.99955 ± 0.00002, Abouchami et al., 2011; Sieber et al., 2019a; Xue et al., 2013) and culture experiments (0.99974 ± 0.00005, Horner et al., 2013).

Assuming that WW represents the initial conditions prior to seasonal uptake, the removal of dCd and change in δ^{114}Cd ($\Delta\delta^{114}$Cd) are correlated, with the highest dCd removal and $\Delta\delta^{114}$Cd corresponding to the highest [chl a]$_{wt.avg}$ (Fig. 8 and Supplementary Fig. S3). This suggests biological uptake predominantly controls both [dCd] and δ^{114}Cd in the surface (e.g., Conway and John, 2015; Janssen et al., 2019; Yang et al., 2018) without evidence of other source influences to the surface layer (see section 4.1 and Tian et al., 2023b). The Amundsen Sea data follows Rayleigh trends more closely, with higher fractionation factors than the Weddell Sea (Fig. 7d, 7e, and 7f), implying distinct biological

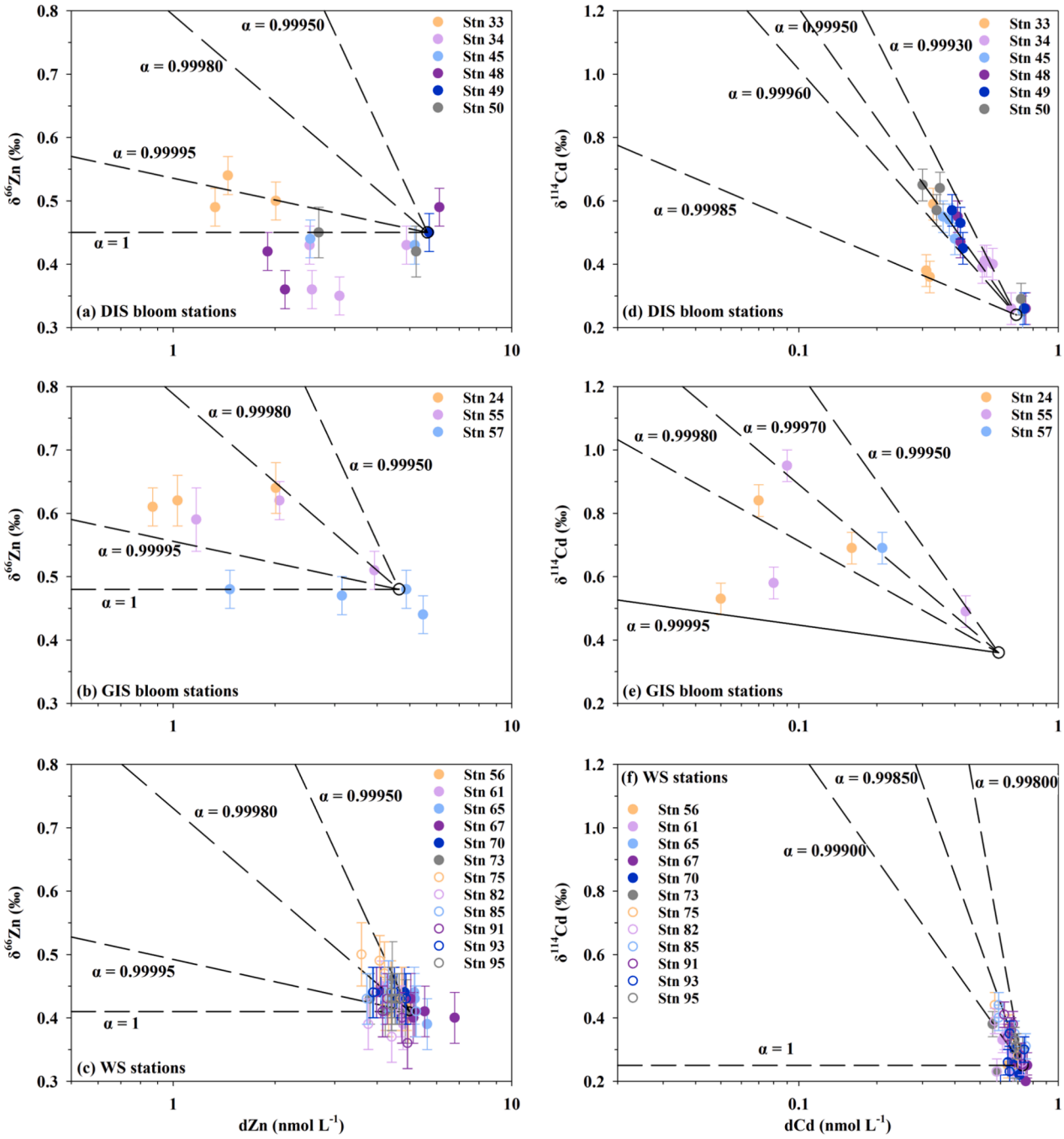

Fig. 7. Isotope systematics of δ^{66}Zn and δ^{114}Cd in the surface layer of the bloom stations of the ANA08B expedition and the WS stations of the PS117 expedition. (a) and (d) DIS bloom stations; (b) and (e) GIS bloom stations; (c) and (f) the WS stations. The dashed lines represent closed-system Rayleigh fractionation trends with $\alpha = R_{biomass}/R_{seawater}$, which are modelled by setting δ^{66}Zn and δ^{114}Cd values in WW as starting points (black open circle). The error bars for δ^{66}Zn and δ^{114}Cd are 2 SD.

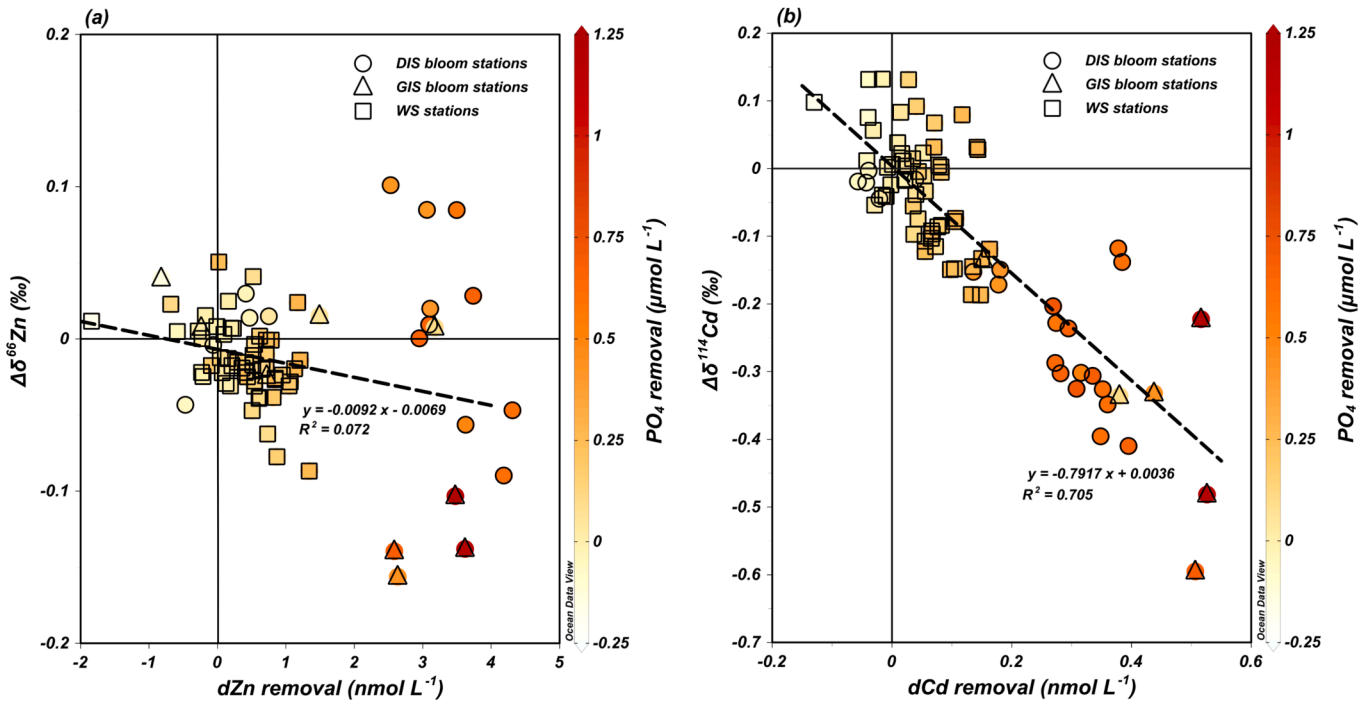

Fig. 8. Correlations of the removal of elements with the change of isotope composition in the surface layer at the bloom stations (ANA08B expedition) and the WS stations (PS117 expedition). Both the removal of elements (concentrations) and the change in isotope composition are calculated as follows: the removal (or change) = observed values – WW values. In the same manner, the color grading shows the removal of PO_4. The dashed lines represent the correlations for all stations combined.

fractionation between regions (Janssen et al., 2017; Xie et al., 2017).

Two plausible explanations (or their combination) may account for this observation. First, different phytoplankton species may exhibit varying fractionation factors, affecting the overall magnitude of fractionation (Abouchami et al., 2011). To date, there is only a handful of culturing studies investigating the fractionation effect of Cd uptake by distinct species – freshwater algae *Chlamydomonas reinhardtii* and *Chlorella* (Lacan et al., 2006), marine flagellate *Dunaliella tertiolecta* (John and Conway, 2014), and heterotrophic bacteria *Escherichia coli* (Horner et al., 2013). These selected species from both marine and freshwater environments seem to generate similar isotope fractionation effects for Cd uptake, and Horner et al. (2013) suggested that metal homeostasis (i.e., Cd sequestration within cells to avoid toxicity), rather than physiological function (e.g., carbonic anhydrase expression), drives δ^{114}Cd in both cultures and nature with no differences between species. However, John and Conway (2014) observed difference in δ^{114}Cd between natural and culture experiments and suggested that phytoplankton species and/or different uptake pathways employed under ambient [dCd] variation may drive variable Cd isotope fractionation. Additionally, different species with distinct elemental requirements under different environmental conditions (e.g., Fe-replete/deplete) (e.g., Ho et al., 2003; Twining and Baines, 2013; Twining et al., 2003) may also affect the uptake of Cd and the subsequent fractionation effects.

In this study, phytoplankton composition differed between the Amundsen Sea and the Weddell Sea – haptophytes (DIS bloom) and diatoms (GIS bloom) dominated in the Amundsen Sea (over 50 % of bulk phytoplankton composition), while the Weddell Sea had a more diverse community (Supplementary Fig. S3). The more uniform Amundsen Sea community follows Rayleigh trends more closely than the mixed Weddell Sea community, which shows more scatter, suggesting different species may indeed have distinct biological fractionation factors. In the Amundsen Sea, fractionation factors for the haptophyte bloom (0.99930 to 0.99960; α derived after excluding two datapoints from Stn 33 that deviated) were lower than for the diatom bloom (0.99970 to 0.99995) (Fig. 7d and 7e), implying haptophytes and diatoms might use different transporters or pathways for Cd uptake, similar to what was speculated for Fe (Tian et al., 2023). Conversely, a mixed phytoplankton community may likely lead to a less clear Rayleigh fractionation trend ('muted' scenario) in the Weddell Sea as the α value is not driven by a single uptake mechanism, but this remains speculation. Although diatoms and haptophytes are the most commonly dominant phytoplankton species in the Southern Ocean, there are limited studies on the variability in Cd fractionation between them, either from in-situ observations or culturing experiments. Further investigations and culturing experiments are needed to understand biological Cd fractionation by these species and its effect on Cd cycling in the surface Southern Ocean.

The second explanation could be the difference in phytoplankton uptake between the Weddell Sea and Amundsen Sea. Lower productivity in the Weddell Sea leads to less isotope fractionation (i.e., remnant dCd closer to the deep ocean signal, Janssen et al., 2017; Xie et al., 2017), as seen in the Weddell Sea. In contrast, greater Cd uptake in the Amundsen Sea results in a heavier remnant dCd pool (Fig. 7). This is supported by higher surface $[\text{chl }\alpha]_{\text{wt.avg}}$ in the Amundsen Sea bloom stations (4.32 ± 1.36 μg L^{-1}) compared to the Weddell Sea (0.13 ± 0.09 μg L^{-1}) (Supplementary Fig. S3), and larger PO_4 and Cd removal in the Amundsen Sea surface layer (Fig. 8).

Overall, the discrepancy in Rayleigh fractionation factors for δ^{114}Cd likely results from a combination of these processes – higher growth in the Amundsen Sea and different uptake mechanisms – leading to distinct patterns in the Amundsen Sea and the Weddell Sea. However, the similar degree of PO_4 and Cd removal between the two Amundsen Sea blooms suggests that species differences may play a key role in controlling fractionation trends.

4.3.2. *δ^{66}Zn systematics in the surface layer: interplay of multiple biogeochemistry processes*

The variation in δ^{66}Zn in both region's surface is less than in δ^{114}Cd – δ^{66}Zn ranged from + 0.35 to + 0.64 ‰ at the Amundsen Sea bloom stations and from + 0.36 to + 0.50 ‰ at the WS stations (Fig. 7a, 7b, 7c). The highest δ^{66}Zn did not consistently correspond to the lowest [dZn],

and the correlation between Zn removal and $\Delta\delta^{66}Zn$ was weaker than for Cd (Fig. 8), despite Zn drawdown exceeding 60 % of the dissolved pool in the surface layer relative to WW. These patterns suggest that $\delta^{66}Zn$ in the surface layer is not predominantly controlled by simple fractionation during biological uptake, even though high labile particulate Zn (Tian et al., 2023b) and increased Zn uptake (Kell et al., 2024) were reported in the Amundsen Sea. This result is also supported by the isotope systematics – most $\delta^{66}Zn$ data did not follow a clear Rayleigh fractionation trend, with both [dZn] and $\delta^{66}Zn$ remaining within a narrow range (Fig. 7a, 7b, 7c), except at Stn 33 (DIS bloom) and Stns 55 and 24 (GIS bloom), with fractionation factors around 0.99995 and between 0.99980 and 0.99995, respectively. These values are consistent with those reported previously for biological uptake in the Southern Ocean (0.99995 ± 0.00001,Sieber et al., 2020; Wang et al., 2019) where Zn uptake causes only slight isotope fractionation, supported by culturing experiments (John et al., 2007; Köbberich and Vance, 2017, 2019). Additionally, despite the presumably small isotope fractionation, the consistent α observed at Stn 33 (DIS) and GIS bloom stations suggest similar Zn fractionation effects during assimilation by haptophytes and diatoms, in contrast to Cd.

The absence of Rayleigh fractionation trends for Zn in most DIS bloom stations and WS stations could result from adsorption (in the case of the Amundsen Sea) and modest biological uptake (in the case of the Weddell Sea). In a recent study, Grun et al. (2023) found a heavy particulate Zn isotope signature in a predominantly diatom community from field incubation experiments at the Southern Ocean Time Series (SOTS) site (47°S; 142°E) following Fe addition, in contrast to the expected uptake of light isotopes. They suggest that increased organic production can enhance the adsorption of isotopically heavy Zn onto cell surfaces, muting isotope fractionation from uptake into the cell and resulting in lower dissolved $\delta^{66}Zn$. Similar effects have been invoked to explain $\delta^{66}Zn$ distributions in other regions by Weber et al. (2018) and Sieber et al. (2023a). Since the Amundsen Sea receives additional Fe from upwelled mCDW and continental sediments (Tian et al., 2023; van Manen et al., 2022), Fe stress is likely alleviated (Eich et al., 2024) and thus analogous to conditions observed by Grun et al. (2023). In contrast, the Weddell Sea is more Fe stressed due to a lack of upwelling (Eich et al., 2024). Lower productivity results in less preferential uptake of light Zn and reduced scavenging of heavy Zn, contributing to a muted signal and the absence of Rayleigh trends in the Weddell Sea surface layer.

Beyond uptake and scavenging, organic complexation also influences the isotope composition of dZn (Köbberich and Vance, 2017; Sieber et al., 2023; Weber et al., 2018). For example, Köbberich and Vance (2017) showed that the organic chelator EDTA preferentially binds isotopically heavy Zn, potentially overprinting biological uptake fractionation. Ligand-induced fractionation may sometimes exceed biological uptake effects (Köbberich and Vance, 2019; Vance et al., 2019). Although Zn ligand measurements were unavailable in this study, the Southern Ocean is known to be enriched in free Zn^{2+} (Baars and Croot, 2011), suggesting ligand-induced fractionation may be less significant here, but further work is needed to confirm this speculation.

5. Implications

The biogeochemistry of bioactive elements such as Zn and Cd in Antarctic marginal seas – particularly the Amundsen and Weddell Seas – may significantly influence the open Southern Ocean and global climate. In the Amundsen Sea, highly productive phytoplankton blooms, triggered by Fe inputs, enhance atmospheric CO_2 uptake (e.g., Alderkamp et al., 2012; Gerringa et al., 2012). The efficiency of carbon uptake by phytoplankton varies depending on species (e.g., Morel et al., 2020; Twining and Baines, 2013) and Fe availability in seawater (e.g., Lane et al., 2009; Twining et al., 2004). Differences in Rayleigh fractionation factors for $\delta^{114}Cd$ between haptophyte- and diatom-dominated blooms observed in this study suggest species-specific uptake mechanisms and/or fractionation effects. In contrast, $\delta^{66}Zn$ shows only modest variability in uptake fractionation, indicating a more limited biological effect and highlighting the role of other processes such as scavenging and organic complexation. While culture studies have examined uptake-related fractionation of $\delta^{114}Cd$ and $\delta^{66}Zn$ (e.g., Horner et al., 2013; John and Conway, 2014; John et al., 2007), this study presents the first field-based assessment of uptake fractionation in near-monospecific blooms (up to 100 % haptophytes and 98 % diatoms), providing new insights into Cd and Zn uptake mechanisms and their role in carbon uptake in the Southern Ocean.

In the Weddell Sea, coastal sources near the Antarctic Peninsula – such as ice melt, upwelling, and sediment resuspension – are thought to supply dZn and dCd to the central gyre (Sañudo-Wilhelmy et al., 2002). Given the hydrographic structure of the western Weddell Sea, the formation of deep waters on the shelf likely entrains these elements, affecting [dZn] and [dCd] in exported waters. However, this study reveals that, beyond external inputs, physical mixing is a key driver of deep-water trace metal distributions. By combining dissolved concentrations and isotope compositions, we demonstrate the dominant role of mixing in setting global deep-water $\delta^{114}Cd$ and $\delta^{66}Zn$, underscoring the broader impact of physical processes in Zn and Cd cycling within the Weddell Sea and global deep waters.

6. Conclusions

In this study, we use $\delta^{66}Zn$ and $\delta^{114}Cd$ to assess the external sources of Zn and Cd and the processes affecting their distributions in two coastal Antarctic systems. Firstly, in the Amundsen Sea, mCDW is the primary Zn and Cd source, characterized by $\delta^{66}Zn$ and $\delta^{114}Cd$ values identical to global deep-water signatures. This signature remains unchanged as mCDW moves over the continental shelf, through the ice shelf cavity, and back, indicating minor contributions from shelf sediments and ice shelf meltwater, consistent with previous [dZn] and [dCd] observations (Tian et al., 2023b).

Secondly, in the Weddell Sea, the shelf station near Antarctic Peninsula shows uniformly lower [dZn] and [dCd], with $\delta^{66}Zn$ and $\delta^{114}Cd$ indistinguishable from deep-water signals in the upper 250 m, implying meltwater is not a significant Zn and Cd source. Strong correlations between dissolved concentrations and S in dense shelf water, pre-WSBW, WDW, and WSDW indicate physical mixing of pre-WSBW with WDW and WSDW as pre-WSBW descends (Fig. 9). Nearly identical $\delta^{66}Zn$ and $\delta^{114}Cd$ values across these water masses and AABW suggest that deep-water signatures are established early during WSBW formation and remain constant as it enters the global ocean. Additionally, a lighter Cd isotope signature (+0.07 ‰) between 250 m and 1500 m in the inner Weddell Gyre, compared to the outer Weddell Gyre (+0.23 ‰), likely results from reduced ventilation and accumulative regeneration within the gyre.

Lastly, in the surface layer, clear closed system Rayleigh fractionation trends for $\delta^{114}Cd$ indicate biological uptake as the predominant control, whereas such trends for $\delta^{66}Zn$ are less clear, likely due to the interplay of biological uptake, adsorption, and perhaps ligand complexation. Fractionation factors (α) for $\delta^{114}Cd$ in the haptophyte bloom (0.99930 to 0.99960) are lower than in the diatom bloom (0.99970 to 0.99995), suggesting different fractionation by haptophytes and diatoms, but this remains speculative. In contrast, similar α values for $\delta^{66}Zn$ at one haptophyte station (0.99995) and in the diatom bloom (0.99980 to 0.99995) suggest similar isotope fractionation effects for Zn assimilation by both species.

This current data highlights the importance of changes in circulation, ventilation, biological activity or particle loading (and thus scavenging intensity) on the biogeochemistry of Cd and Zn in coastal Antarctic regions. Given the strong connection of the Amundsen Sea (e.g., outflowing mCDW) and the Weddell Sea (e.g., AABW formation) to the global ocean, such observations provide insights into the impacts of regional coastal systems on the global Zn and Cd cycling.

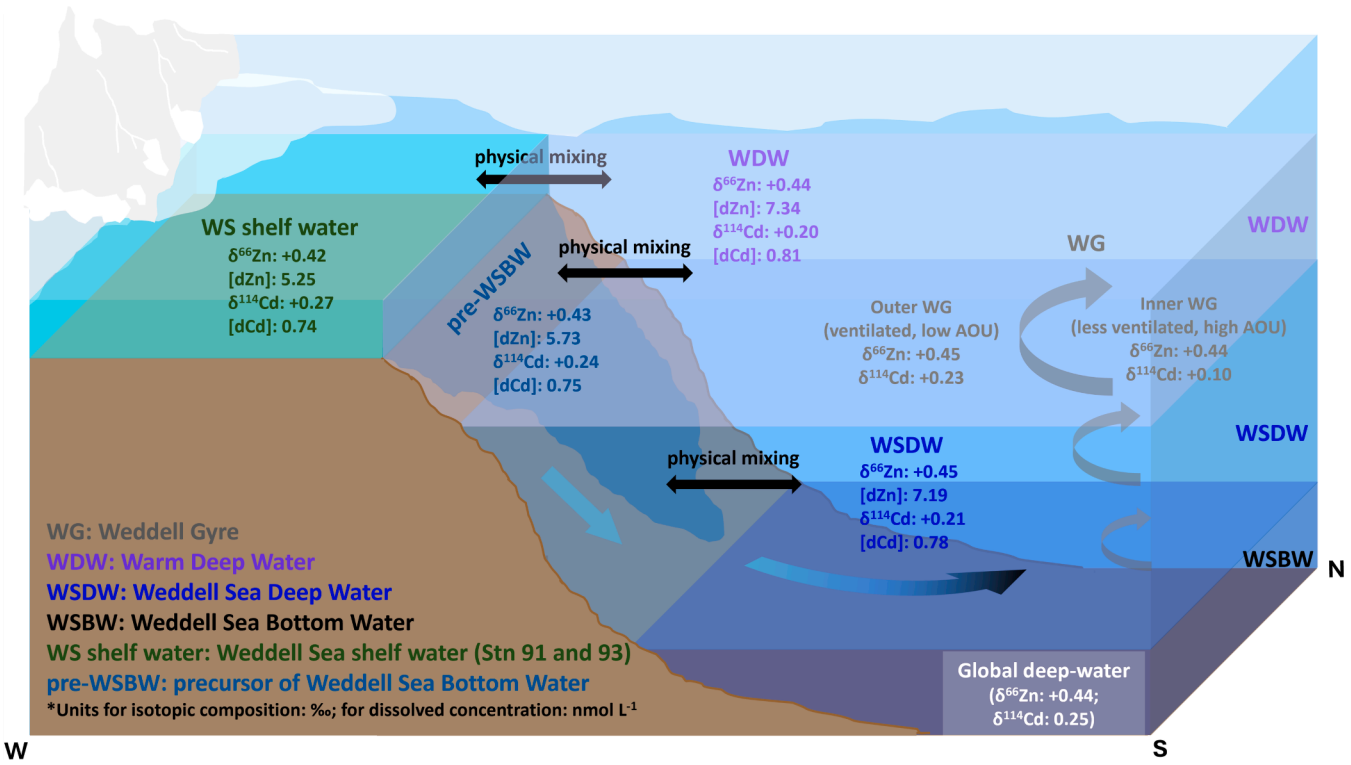

Fig. 9. Schematic of δ^{66}Zn and δ^{114}Cd in different water masses in the Weddell Sea. All values are obtained from this study except for the global deep water values are derived from previous studies (for δ^{66}Zn: Bermin et al., 2006; Conway and John, 2014; Lemaitre et al., 2020; Sieber et al., 2020; Sieber et al., 2023; Takano et al., 2017; for δ^{114}Cd: Abouchami et al., 2014; Conway and John, 2015; George et al., 2019; Xie et al., 2017). The schematic is for illustration purposes only and are not to scale.

Data availability

Data are available through NIOZ Dataverse at https://doi.org/10.25850/nioz/7b.b.bd.

CRediT authorship contribution statement

Hung-An Tian: Writing – original draft, Visualization, Validation, Investigation, Conceptualization. **Mathijs van Manen:** Investigation. **Charlotte Eich:** Investigation. **Jinyoung Jung:** Investigation. **Willem H.v.d. Poll:** Investigation. **Gert-Jan Reichart:** Supervision, Resources. **Tim M. Conway:** Investigation. **Rob Middag:** Writing – review & editing, Validation, Supervision, Project administration, Investigation, Funding acquisition, Conceptualization.

Declaration of competing interest

The authors declare that they have no known competing financial interests or personal relationships that could have appeared to influence the work reported in this paper.

Acknowledgments

This work was supported by the Dutch Research Council (NWO) (grant number: ALWPP.2016.020 to RM) and the International GEOTRACES Programme is possible in part thanks to the support from the U. S. National Science Foundation (Grant OCE2123354 to TMC) to the Scientific Committee on Oceanic Research (SCOR). Expedition ANA08B (project number: PE24110) with the R/V Araon was supported by the Korea Polar Research Institute (KOPRI) and our participation in R/V Polarstern expedition PS117 was funded by AWI (under grant number: AWI_PS117_02). We thank the captain and the crew of the R/V Araon and R/V Polarstern (AWI, 2017), as well as the expedition leaders SangHoon Lee and Olaf Boebel and all the scientists on board, for their assistance and support during the expeditions. We thank Sharyn Ossebaar for nutrient analysis; Piet van Gaever for oxygen isotope analysis; Patrick Lann for discussion of trace metal data; Corina Brussaard for data supervision and interpretation; Matthias Sieber for assistance with MC-ICP-MS analytical calculations, as well as Sven Ober and colleagues from NIOZ National Marine Facilities (NMF) for the preparation of Titan CTD and other facilities used during this expedition. Piet ter Schure and his team from DMT Marine Equipment are acknowledged for their great help with the winch setup for the Titan sampling system used on R/V Araon. We also thank M. Tian for valuable discussions and advice.

Appendix A. Supplementary material

This supplementary material includes Acronym list; S1 (Analytical pretreatment – extraction and purification); S2 (Double spike preparation); S3 (Mass balance model for freshwater input calculation); Table S1 (Extraction and purification procedure implemented in this study); Table S2 (Instrumental settings for Zn and Cd isotope analysis on Thermo Neptune Plus Multi-Collector ICPMS); Fig. S1 (Elution profile and recovery of the purification procedure in Table S1); Fig. S2 (Procedural test of extraction and purification for Zn and Cd isotope analysis and comparison with

previously reported values); Fig. S3 (Weighted average of [chl *a*] ([chl *a*]$_{wt.avg}$) and phytoplankton community composition of all ANA08B (the Amundsen Sea) and PS117 (the Weddell Sea) stations; Fig. S4 (Estimated fraction of meteoric water (f_{met}) of the shelf stations along the Weddell Sea transect); Fig. S5 (Linear regression of dissolved elemental concentrations derived from ICPMS (Element 2) versus concentrations derived from ICPMS (Neptune Plus) for [dZn] and [dCd]).

Supplementary material to this article can be found online at https://doi.org/10.1016/j.gca.2025.04.017.

References

Abouchami, W., Galer, S.J.G., de Baar, H.J.W., Alderkamp, A.C., Middag, R., Laan, P., Feldmann, H., Andreae, M.O., 2011. Modulation of the Southern Ocean cadmium isotope signature by ocean circulation and primary productivity. Earth and Planetary Science Letters 305 (1), 83–91.

Abouchami, W., Galer, S.J.G., de Baar, H.J.W., Middag, R., Vance, D., Zhao, Y., Klunder, M., Mezger, K., Feldmann, H., Andreae, M.O., 2014. Biogeochemical cycling of cadmium isotopes in the Southern Ocean along the Zero Meridian. Geochimica et Cosmochimica Acta 127, 348–367.

Alderkamp, A.-C., Mills, M.M., van Dijken, G.L., Laan, P., Thuróczy, C.-E., Gerringa, L.J. A., de Baar, H.J.W., Payne, C.D., Visser, R.J.W., Buma, A.G.J., Arrigo, K.R., 2012. Iron from melting glaciers fuels phytoplankton blooms in the Amundsen Sea (Southern Ocean): Phytoplankton characteristics and productivity. Deep Sea Research Part II: Topical Studies in Oceanography 71–76, 32–48.

Archer, C., Andersen, M.B., Cloquet, C., Conway, T.M., Dong, S., Ellwood, M., Moore, R., Nelson, J., Rehkämper, M., Rouxel, O., Samanta, M., Shin, K.-C., Sohrin, Y., Takano, S., Wasylenki, L., 2017. Inter-calibration of a proposed new primary reference standard AA-ETH Zn for zinc isotopic analysis. Journal of Analytical Atomic Spectrometry 32 (2), 415–419.

Arrigo, K.R., Lowry, K.E., van Dijken, G.L., 2012. Annual changes in sea ice and phytoplankton in polynyas of the Amundsen Sea, Antarctica. Deep Sea Research Part II: Topical Studies in Oceanography 71–76, 5–15.

Arrigo, K.R., van Dijken, G.L., 2003. Phytoplankton dynamics within 37 Antarctic coastal polynya systems. Journal of Geophysical Research: Oceans 108 (C8), 3271.

Awi, 2017. Polar Research and Supply Vessel POLARSTERN Operated by the Alfred-Wegener-Institute. Journal of Large-Scale Research Facilities 3, A119.

Baars, O., Abouchami, W., Galer, S.J.G., Boye, M., Croot, P.L., 2014. Dissolved cadmium in the Southern Ocean: Distribution, speciation, and relation to phosphate. Limnology and Oceanography 59 (2), 385–399.

Baars, O., Croot, P.L., 2011. The speciation of dissolved zinc in the Atlantic sector of the Southern Ocean. Deep Sea Research Part II: Topical Studies in Oceanography 58 (25), 2720–2732.

Bermin, J., Vance, D., Archer, C., Statham, P.J., 2006. The determination of the isotopic composition of Cu and Zn in seawater. Chemical Geology 226 (3), 280–297.

Bruland, K.W., 1980. Oceanographic distributions of cadmium, zinc, nickel, and copper in the North Pacific. Earth and Planetary Science Letters 47 (2), 176–198.

Bruland, K.W., Middag, R., Lohan, M.C., 2014. Controls of Trace Metals in Seawater. In: Holland, H.D., Turekian, K.K. (Eds.), Treatise on Geochemistry (second Edition). Elsevier, Oxford, pp. 19–51.

Bryan, A.L., Dickson, A.J., Dowdall, F., Homoky, W.B., Porcelli, D., Henderson, G.M., 2021. Controls on the cadmium isotope composition of modern marine sediments. Earth and Planetary Science Letters 565, 116946.

Chen, L., Little, S.H., Kreissig, K., Severmann, S., McManus, J., 2021. Isotopically Light Cd in Sediments Underlying Oxygen Deficient Zones. Frontiers in Earth Science 9.

Cloquet, C., Carignan, J., Libourel, G., Sterckeman, T., Perdrix, E., 2006. Tracing Source Pollution in Soils Using Cadmium and Lead Isotopes. Environmental Science & Technology 40 (8), 2525–2530.

Conway, T.M., Horner, T.J., Plancherel, Y., González, A.G., 2021. A decade of progress in understanding cycles of trace elements and their isotopes in the oceans. Chemical Geology 580, 120381.

Conway, T.M., John, S.G., 2014. The biogeochemical cycling of zinc and zinc isotopes in the North Atlantic Ocean. Global Biogeochemical Cycles 28 (10), 1111–1128.

Conway, T.M., John, S.G., 2015. The cycling of iron, zinc and cadmium in the North East Pacific Ocean – Insights from stable isotopes. Geochimica et Cosmochimica Acta 164, 262–283.

Conway, T.M., Rosenberg, A.D., Adkins, J.F., John, S.G., 2013. A new method for precise determination of iron, zinc and cadmium stable isotope ratios in seawater by double-spike mass spectrometry. Analytica Chimica Acta 793, 44–52.

Croot, P.L., Baars, O., Streu, P., 2011. The distribution of dissolved zinc in the Atlantic sector of the Southern Ocean. Deep Sea Research Part II: Topical Studies in Oceanography 58 (25), 2707–2719.

Donnelly, M., Leach, H., Strass, V., 2017. Modification of the deep salinity-maximum in the Southern Ocean by circulation in the Antarctic Circumpolar Current and the Weddell Gyre. Ocean Dynamics 67 (7), 813–838.

Dutrieux, P., De Rydt, J., Jenkins, A., Holland, P.R., Ha, H.K., Lee, S.H., Steig, E.J., Ding, Q., Abrahamsen, E.P., Schröder, M., 2014. Strong Sensitivity of Pine Island Ice-Shelf Melting to Climatic Variability. Science 343 (6167), 174.

Eich, C., Biggs, T.E.G., van de Poll, W.H., van Manen, M., Tian, H.-A., Jung, J., Lee, Y., Middag, R., Brussaard, C.P.D., 2022. Ecological Importance of Viral Lysis as a Loss Factor of Phytoplankton in the Amundsen Sea, Microorganisms.

Eich, C., van Manen, M., McCain, J.S.P., Jabre, L.J., van de Poll, W.H., Jung, J., Pont, S.B. E.H., Tian, H.A., Ardiningsih, I., Reichart, G.J., Bertrand, E.M., Brussaard, C.P.D., Middag, R., 2024. Temperature-enhanced effects of iron on Southern Ocean phytoplankton. Egusphere 2024, 1–45.

Ellwood, M.J., Strzepek, R.F., Strutton, P.G., Trull, T.W., Fourquez, M., Boyd, P.W., 2020. Distinct iron cycling in a Southern Ocean eddy. Nature Communications 11 (1), 825.

Fahrbach, E., Hoppema, M., Rohardt, G., Schröder, M., Wisotzki, A., 2004. Decadal-scale variations of water mass properties in the deep Weddell Sea. Ocean Dynamics 54 (1), 77–91.

Fahrbach, E., Peterson, R.G., Rohardt, G., Schlosser, P., Bayer, R., 1994. Suppression of bottom water formation in the southeastern Weddell sea. Deep Sea Research Part i: Oceanographic Research Papers 41 (2), 389–411.

Field, C.B., Behrenfeld, M.J., Randerson, J.T., Falkowski, P., 1998. Primary Production of the Biosphere: Integrating Terrestrial and Oceanic Components. Science 281 (5374), 237–240.

Foldvik, A., Gammelsrød, T., Tørresen, T., 1985. Circulation and Water Masses on the Southern Weddell Sea Shelf. Oceanology of the Antarctic Continental Shelf. 5–20.

Foster, T.D., Carmack, E.C., 1976. Frontal zone mixing and Antarctic Bottom water formation in the southern Weddell Sea. Deep Sea Research and Oceanographic Abstracts 23 (4), 301–317.

Gault-Ringold, M., Adu, T., Stirling, C.H., Frew, R.D., Hunter, K.A., 2012. Anomalous biogeochemical behavior of cadmium in subantarctic surface waters: Mechanistic constraints from cadmium isotopes. Earth and Planetary Science Letters 341–344, 94–103.

George, E., Stirling, C.H., Gault-Ringold, M., Ellwood, M.J., Middag, R., 2019. Marine biogeochemical cycling of cadmium and cadmium isotopes in the extreme nutrient-depleted subtropical gyre of the South West Pacific Ocean. Earth and Planetary Science Letters 514, 84–95.

Gerringa, L.J.A., Alderkamp, A.-C., Laan, P., Thuróczy, C.-E., De Baar, H.J.W., Mills, M. M., van Dijken, G.L., Haren, Arrigo, H.V., 2012. Iron from melting glaciers fuels the phytoplankton blooms in Amundsen Sea (Southern Ocean): Iron biogeochemistry. Deep Sea Research Part II: Topical Studies in Oceanography 71–76, 16–31.

Gerringa, L.J.A., Alderkamp, A.-C., Laan, P., Thuróczy, C.-E., De Baar, H.J.W., Mills, M. M., van Dijken, G.L., Haren, H.v., Arrigo, K.R., 2020. Corrigendum to "Iron from melting glaciers fuels the phytoplankton blooms in Amundsen Sea (Southern Ocean): iron biogeochemistry" (Gerringa et al., 2012). Deep Sea Research Part II: Topical Studies in Oceanography 177, 104843. Doi: 10.1016/j.dsr2.2020.104843.

Gerringa, L.J.A., Laan, P., Arrigo, K.R., van Dijken, G.L., Alderkamp, A.C., 2019. The organic complexation of iron in the Ross sea. Marine Chemistry 215, 103672.

Gordon, A.L., Visbeck, M., Huber, B., 2001. Export of Weddell Sea deep and bottom water. Journal of Geophysical Research: Oceans 106 (C5), 9005–9017.

Gourmelen, N., Goldberg, D.N., Snow, K., Henley, S.F., Bingham, R.G., Kimura, S., Hogg, A.E., Shepherd, A., Mouginot, J., Lenaerts, J.T.M., Ligtenberg, S.R.M., van de Berg, W.J., 2017. Channelized Melting Drives Thinning Under a Rapidly Melting Antarctic Ice Shelf. Geophysical Research Letters 44 (19), 9796–9804.

Grun, R., Samanta, M., Ellwood, M.J., 2023. Variability in zinc:phosphorous and zinc: silicon ratios and zinc isotope fractionation in Southern Ocean diatoms: Observations from laboratory and field experiments. Marine Chemistry 257, 104330.

Guinoiseau, D., Galer, S.J.G., Abouchami, W., Frank, M., Achterberg, E.P., Haug, G.H., 2019. Importance of Cadmium Sulfides for Biogeochemical Cycling of Cd and Its Isotopes in Oxygen Deficient Zones—A Case Study of the Angola Basin. Global Biogeochemical Cycles 33 (12), 1746–1763.

Ho, T.-Y., Quigg, A., Finkel, Z.V., Milligan, A.J., Wyman, K., Falkowski, P.G., Morel, F.M. M., 2003. THE ELEMENTAL COMPOSITION OF SOME MARINE PHYTOPLANKTON1. Journal of Phycology 39 (6), 1145–1159.

Horner, T.J., Lee, R.B.Y., Henderson, G.M., Rickaby, R.E.M., 2013. Nonspecific uptake and homeostasis drive the oceanic cadmium cycle. Proceedings of the National Academy of Sciences 110 (7), 2500–2505.

Horner, T.J., Little, S.H., Conway, T.M., Farmer, J.R., Hertzberg, J.E., Janssen, D.J., Lough, A.J.M., McKay, J.L., Tessin, A., Galer, S.J.G., Jaccard, S.L., Lacan, F., Paytan, A., Wuttig, K., Geotraces–Pages Biological Productivity Working Group Members, 2021. Bioactive Trace Metals and Their Isotopes as Paleoproductivity Proxies: An Assessment Using GEOTRACES-Era Data. Global Biogeochemical Cycles 35 (11), e2020GB006814.

Huhn, O., Hellmer, H.H., Rhein, M., Rodehacke, C., Roether, W., Schodlok, M.P., Schröder, M., 2008. Evidence of deep- and bottom-water formation in the western Weddell Sea. Deep Sea Research Part II: Topical Studies in Oceanography 55 (8), 1098–1116.

Jacobs, S., Jenkins, A., Hellmer, H., Giulivi, C., Nitsche, F., Huber, B., Guerrero, R., 2012. THE AMUNDSEN SEA AND THE ANTARCTIC ICE SHEET. Oceanography 25 (3), 154–163.

Jacobs, S.S., Hellmer, H.H., Jenkins, A., 1996. Antarctic Ice Sheet melting in the southeast Pacific. Geophysical Research Letters 23 (9), 957–960.

Janssen, D.J., Abouchami, W., Galer, S.J.G., Cullen, J.T., 2017. Fine-scale spatial and interannual cadmium isotope variability in the subarctic northeast Pacific. Earth and Planetary Science Letters 472, 241–252.

Janssen, D.J., Abouchami, W., Galer, S.J.G., Purdon, K.B., Cullen, J.T., 2019. Particulate cadmium stable isotopes in the subarctic northeast Pacific reveal dynamic Cd cycling and a new isotopically light Cd sink. Earth and Planetary Science Letters 515, 67–78.

Janssen, D.J., Sieber, M., Ellwood, M.J., Conway, T.M., Barrett, P.M., Chen, X., de Souza, G.F., Hassler, C.S., Jaccard, S.L., 2020. Trace metal and nutrient dynamics

across broad biogeochemical gradients in the Indian and Pacific sectors of the Southern Ocean. Marine Chemistry 221, 103773.
John, S.G., Conway, T.M., 2014. A role for scavenging in the marine biogeochemical cycling of zinc and zinc isotopes. Earth and Planetary Science Letters 394, 159–167.
John, S.G., Geis, R.W., Saito, M.A., Boyle, E.A., 2007. Zinc isotope fractionation during high-affinity and low-affinity zinc transport by the marine diatom Thalassiosira oceanica. Limnology and Oceanography 52 (6), 2710–2714.
John, S.G., Helgoe, J., Townsend, E., 2018. Biogeochemical cycling of Zn and Cd and their stable isotopes in the Eastern Tropical South Pacific. Marine Chemistry 201, 256–262.
Jullion, L., Garabato, A.C.N., Bacon, S., Meredith, M.P., Brown, P.J., Torres-Valdés, S., Speer, K.G., Holland, P.R., Dong, J., Bakker, D., Hoppema, M., Loose, B., Venables, H.J., Jenkins, W.J., Messias, M.-J., Fahrbach, E., 2014. The contribution of the Weddell Gyre to the lower limb of the Global Overturning Circulation. Journal of Geophysical Research: Oceans 119 (6), 3357–3377.
Kell, R.M., Chmiel, R.J., Rao, D., Moran, D.M., McIlvin, M.R., Horner, T.J., Schanke, N.L., Dunbar, R.B., DiTullio, G.R., Saito, M.A., 2024. High metabolic zinc demand within native Amundsen and Ross Sea phytoplankton communities determined by stable isotope uptake rate measurements. Egusphere 2024, 1–55.
Kim, T.-W., Yang, H.W., Dutrieux, P., Wåhlin, A.K., Jenkins, A., Kim, Y.G., Ha, H.K., Kim, C.-S., Cho, K.-H., Park, T., Park, J., Lee, S., Cho, Y.-K., 2021. Interannual Variation of Modified Circumpolar Deep Water in the Dotson-Getz Trough, West Antarctica. Journal of Geophysical Research: Oceans 126 (12), e2021JC017491.
Klatt, O., Fahrbach, E., Hoppema, M., Rohardt, G., 2005. The transport of the Weddell Gyre across the Prime Meridian. Deep Sea Research Part II: Topical Studies in Oceanography 52 (3), 513–528.
Köbberich, M., Vance, D., 2017. Kinetic control on Zn isotope signatures recorded in marine diatoms. Geochimica et Cosmochimica Acta 210, 97–113.
Köbberich, M., Vance, D., 2018. Zinc association with surface-bound iron-hydroxides on cultured marine diatoms: A zinc stable isotope perspective. Marine Chemistry 202, 1–11.
Köbberich, M., Vance, D., 2019. Zn isotope fractionation during uptake into marine phytoplankton: Implications for oceanic zinc isotopes. Chemical Geology 523, 154–161.
Lacan, F., Francois, R., Ji, Y., Sherrell, R.M., 2006. Cadmium isotopic composition in the ocean. Geochimica et Cosmochimica Acta 70 (20), 5104–5118.
Lambelet, M., Rehkämper, M., van de Flierdt, T., Xue, Z., Kreissig, K., Coles, B., Porcelli, D., Andersson, P., 2013. Isotopic analysis of Cd in the mixing zone of Siberian rivers with the Arctic Ocean—New constraints on marine Cd cycling and the isotope composition of riverine Cd. Earth and Planetary Science Letters 361, 64–73.
Lane, E.S., Semeniuk, D.M., Strzepek, R.F., Cullen, J.T., Maldonado, M.T., 2009. Effects of iron limitation on intracellular cadmium of cultured phytoplankton: Implications for surface dissolved cadmium to phosphate ratios. Marine Chemistry 115 (3), 155–162.
Lemaitre, N., de Souza, G.F., Archer, C., Wang, R.-M., Planquette, H., Sarthou, G., Vance, D., 2020. Pervasive sources of isotopically light zinc in the North Atlantic Ocean. Earth and Planetary Science Letters 539, 116216.
Liao, W.-H., Takano, S., Yang, S.-C., Huang, K.-F., Sohrin, Y., Ho, T.-Y., 2020. Zn Isotope Composition in the Water Column of the Northwestern Pacific Ocean: The Importance of External Sources. Global Biogeochemical Cycles 34 (1), e2019GB006379.
Little, S.H., Vance, D., McManus, J., Severmann, S., 2016. Key role of continental margin sediments in the oceanic mass balance of Zn and Zn isotopes. Geology 44 (3), 207–210.
Little, S.H., Vance, D., Walker-Brown, C., Landing, W.M., 2014. The oceanic mass balance of copper and zinc isotopes, investigated by analysis of their inputs, and outputs to ferromanganese oxide sediments. Geochimica et Cosmochimica Acta 125, 673–693.
Marinov, I., Gnanadesikan, A., Toggweiler, J.R., Sarmiento, J.L., 2006. The Southern Ocean biogeochemical divide. Nature 441 (7096), 964–967.
Martin, J.H., Fitzwater, S.E., Gordon, R.M., 1990. Iron deficiency limits phytoplankton growth in Antarctic waters. Global Biogeochemical Cycles 4 (1), 5–12.
Middag, R., de Baar, H.J.W., Bruland, K.W., 2019. The Relationships Between Dissolved Zinc and Major Nutrients Phosphate and Silicate Along the GEOTRACES GA02 Transect in the West Atlantic Ocean. Global Biogeochemical Cycles 33 (1), 63–84.
Middag, R., de Baar, H.J.W., Klunder, M.B., Laan, P., 2013. Fluxes of dissolved aluminum and manganese to the Weddell Sea and indications for manganese co-limitation. Limnology and Oceanography 58 (1), 287–300.
Middag, R., van Heuven, S.M.A.C., Bruland, K.W., de Baar, H.J.W., 2018. The relationship between cadmium and phosphate in the Atlantic Ocean unravelled. Earth and Planetary Science Letters 492, 79–88.
Miles, T., Lee, S.H., Wåhlin, A., Ha, H.K., Kim, T.W., Assmann, K.M., Schofield, O., 2016. Glider observations of the Dotson Ice Shelf outflow. Deep Sea Research Part II: Topical Studies in Oceanography 123, 16–29.
Moeller, K., Schoenberg, R., Pedersen, R.-B., Weiss, D., Dong, S., 2012. Calibration of the New Certified Reference Materials ERM-AE633 and ERM-AE647 for Copper and IRMM-3702 for Zinc Isotope Amount Ratio Determinations. Geostandards and Geoanalytical Research 36 (2), 177–199.
Morel, F.M.M., Lam, P.J., Saito, M.A., 2020. Trace Metal Substitution in Marine Phytoplankton. Annual Review of Earth and Planetary Sciences 48 (1), 491–517.
Morel, F.M.M., Reinfelder, J.R., Roberts, S.B., Chamberlain, C.P., Lee, J.G., Yee, D., 1994. Zinc and carbon co-limitation of marine phytoplankton. Nature 369 (6483), 740–742.
Nicholls, K.W., Østerhus, S., Makinson, K., Gammelsrød, T., Fahrbach, E., 2009. Ice-ocean processes over the continental shelf of the southern Weddell Sea, Antarctica: A review. Reviews of Geophysics 47 (3).
Nolting, R.F., de Baar, H.J.W., 1994. Behaviour of nickel, copper, zinc and cadmium in the upper 300 m of a transect in the Southern Ocean (57°–62°S, 49°W). Marine Chemistry 45 (3), 225–242.
Nolting, R.F., De Baar, H.J.W., Van Bennekom, A.J., Masson, A., 1991. Cadmium, copper and iron in the Scotia Sea, Weddell Sea and Weddell/Scotia Confluence (Antarctica). Marine Chemistry 35 (1), 219–243.
Orsi, A.H., Johnson, G.C., Bullister, J.L., 1999. Circulation, mixing, and production of Antarctic Bottom Water. Progress in Oceanography 43 (1), 55–109.
Orsi, A.H., Smethie Jr, W.M., Bullister, J.L., 2002. On the total input of Antarctic waters to the deep ocean: A preliminary estimate from chlorofluorocarbon measurements. Journal of Geophysical Research: Oceans 107(C8), 31-31-31-14. Doi: 10.1029/2001JC000976.
Park, H., Song, B., Morel, F.M.M., 2007. Diversity of the cadmium-containing carbonic anhydrase in marine diatoms and natural waters. Environmental Microbiology 9 (2), 403–413.
Planquette, H., Sherrell, R.M., Stammerjohn, S., Field, M.P., 2013. Particulate iron delivery to the water column of the Amundsen Sea, Antarctica. Marine Chemistry 153, 15–30.
Price, N.M., Morel, F.M.M., 1990. Cadmium and cobalt substitution for zinc in a marine diatom. Nature 344 (6267), 658–660.
Randall-Goodwin., Meredith., M.P., Jenkins., A., L.Yager., P., Sherrell., R.M., Abrahamsen., E.P., Guerrero., R., Yuan., X., Mortlock., R.A., Gavahan., K., Alderkamp., A.-C., Ducklow., H., R.Robertson., Stammerjohn., S.E., 2015. Freshwater distributions and water mass structure in the Amundsen Sea Polynya region, Antarctica. Elementa: Science of the Anthropocene 3, 000065. doi.org/doi: 10.12952/journal.elementa.000065.
Ratié, G., Chrastný, V., Guinoiseau, D., Marsac, R., Vaňková, Z., Komárek, M., 2021. Cadmium Isotope Fractionation during Complexation with Humic Acid. Environmental Science & Technology 55 (11), 7430–7444.
Reeve, K.A., Boebel, O., Kanzow, T., Strass, V., Rohardt, G., Fahrbach, E., 2016. A gridded data set of upper-ocean hydrographic properties in the Weddell Gyre obtained by objective mapping of Argo float measurements. Earth Syst. Sci. Data 8 (1), 15–40.
Rehkämper, M., Schönbächler, M., Andreasen, R., 2012. Application of Multiple-Collector Inductively Coupled Plasma Mass Spectrometry to Isotopic Analysis in Cosmochemistry, Isotopic Analysis. pp. 275-315. Doi: 10.1002/9783527650484.ch10.
Ripperger, S., Rehkämper, M., Porcelli, D., Halliday, A.N., 2007. Cadmium isotope fractionation in seawater — A signature of biological activity. Earth and Planetary Science Letters 261 (3), 670–684.
Samanta, M., Ellwood, M.J., Sinoir, M., Hassler, C.S., 2017. Dissolved zinc isotope cycling in the Tasman Sea, SW Pacific Ocean. Marine Chemistry 192, 1–12.
Samanta, M., Ellwood, M.J., Strzepek, R.F., 2018. Zinc isotope fractionation by Emiliania huxleyi cultured across a range of free zinc ion concentrations. Limnology and Oceanography 63 (2), 660–671.
Sañudo-Wilhelmy, S.A., Olsen, K.A., Scelfo, J.M., Foster, T.D., Flegal, A.R., 2002. Trace metal distributions off the Antarctic Peninsula in the Weddell Sea. Marine Chemistry 77 (2), 157–170.
Schlitzer, R., 2020. Ocean Data View.
Schlitzer, R., Anderson, R.F., Dodas, E.M., Lohan, M., Geibert, W., Tagliabue, A., Bowie, A., Jeandel, C., Maldonado, M.T., Landing, W.M., Cockwell, D., Abadie, C., Abouchami, W., Achterberg, E.P., Agather, A., Aguliar-Islas, A., van Aken, H.M., Andersen, M., Archer, C., Auro, M., de Baar, H.J., Baars, O., Baker, A.R., Bakker, K., Basak, C., Baskaran, M., Bates, N.R., Bauch, D., van Beek, P., Behrens, M.K., Black, E., Bluhm, K., Bopp, L., Bouman, H., Bowman, K., Bown, J., Boyd, P., Boye, M., Boyle, E.A., Branellec, P., Bridgestock, L., Brissebrat, G., Browning, T., Bruland, K.W., Brumsack, H.-J., Brzezinski, M., Buck, C.S., Buck, K.N., Buesseler, K., Bull, A., Butler, E., Cai, P., Mor, P.C., Cardinal, D., Carlson, C., Carrasco, G., Casacuberta, N., Casciotti, K.L., Castrillejo, M., Chamizo, E., Chance, R., Charette, M. A., Chaves, J.E., Cheng, H., Chever, F., Christl, M., Church, T.M., Closset, I., Colman, A., Conway, T.M., Cossa, D., Croot, P., Cullen, J.T., Cutter, G.A., Daniels, C., Dehairs, F., Deng, F., Dieu, H.T., Duggan, B., Dulaquais, G., Dumousseaud, C., Echegoyen-Sanz, Y., Edwards, R.L., Ellwood, M., Fahrbach, E., Fitzsimmons, J.N., Russell Flegal, A., Fleisher, M.Q., van de Flierdt, T., Frank, M., Friedrich, J., Fripiat, F., Fröllje, H., Galer, S.J.G., Gamo, T., Ganeshram, R.S., Garcia-Orellana, J., Garcia-Solsona, E., Gault-Ringold, M., George, E., Gerringa, L.J.A., Gilbert, M., Godoy, J.M., Goldstein, S.L., Gonzalez, S.R., Grissom, K., Hammerschmidt, C., Hartman, A., Hassler, C.S., Hathorne, E.C., Hatta, M., Hawco, N., Hayes, C.T., Heimbürger, L.-E., Helgoe, J., Heller, M., Henderson, G.M., Henderson, P.B., van Heuven, S., Ho, P., Horner, T.J., Hsieh, Y.-T., Huang, K.-F., Humphreys, M.P., Isshiki, K., Jacquot, J.E., Janssen, D.J., Jenkins, W.J., John, S., Jones, E.M., Jones, J. L., Kadko, D.C., Kayser, R., Kenna, T.C., Khondoker, R., Kim, T., Kipp, L., Klar, J.K., Klunder, M., Kretschmer, S., Kumamoto, Y., Laan, P., Labatut, M., Lacan, F., Lam, P. J., Lambelet, M., Lamborg, C.H., Le Moigne, F.A.C., Le Roy, E., Lechtenfeld, O.J., Lee, J.-M., Lherminier, P., Little, S., López-Lora, M., Lu, Y., Masque, P., Mawji, E., McClain, C.R., Measures, C., Mehic, S., Barraqueta, J.-L.-M., van der Merwe, P., Middag, R., Mieruch, S., Milne, A., Minami, T., Moffett, J.W., Moncoiffe, G., Moore, W.S., Morris, P.J., Morton, P.L., Nakaguchi, Y., Nakayama, N., Niedermiller, J., Nishioka, J., Nishiuchi, A., Noble, A., Obata, H., Ober, S., Ohnemus, D.C., van Ooijen, J., O'Sullivan, J., Owens, S., Pahnke, K., Paul, M., Pavia, F., Pena, L.D., Peters, B., Planchon, F., Planquette, H., Pradoux, C., Puigcorbé, V., Quay, P., Queroue, F., Radic, A., Rauschenberg, S., Rehkämper, M., Rember, R., Remenyi, T., Resing, J.A., Rickli, J., Rigaud, S., Rijkenberg, M.J.A., Rintoul, S., Robinson, L.F., Roca-Martí, M., Rodellas, V., Roeske, T., Rolison, J.M., Rosenberg, M., Roshan, S., Rutgers van der Loeff, M.M., Ryabenko, E., Saito, M.A., Salt, L.A., Sanial, V., Sarthou, G., Schallenberg, C., Schauer, U., Scher, H.,

Schlosser, C., Schnetger, B., Scott, P., Sedwick, P.N., Semiletov, I., Shelley, R., Sherrell, R.M., Shiller, A.M., Sigman, D.M., Singh, S.K., Slagter, H.A., Slater, E., Smethie, W.M., Snaith, H., Sohrin, Y., Sohst, B., Sonke, J.E., Speich, S., Steinfeldt, R., Stewart, G., Stichel, T., Stirling, C.H., Stutsman, J., Swarr, G.J., Swift, J.H., Thomas, A., Thorne, K., Till, C.P., Till, R., Townsend, A.T., Townsend, E., Tuerena, R., Twining, B.S., Vance, D., Velazquez, S., Venchiarutti, C., Villa-Alfageme, M., Vivancos, S.M., Voelker, A.H.L., Wake, B., Warner, M.J., Watson, R., van Weerlee, E., Alexandra Weigand, M., Weinstein, Y., Weiss, D., Wisotzki, A., Woodward, E.M.S., Wu, J., Wu, Y., Wuttig, K., Wyatt, N., Xiang, Y., Xie, R.C., Xue, Z., Yoshikawa, H., Zhang, J., Zhang, P., Zhao, Y., Zheng, L., Zheng, X.-Y., Zieringer, M., Zimmer, L.A., Ziveri, P., Zunino, P., Zurbrick, C., 2018. The GEOTRACES Intermediate Data Product 2017. Chemical Geology 493, 210–223.

Schmitt, A.-D., Galer, S.J.G., Abouchami, W., 2009. Mass-dependent cadmium isotopic variations in nature with emphasis on the marine environment. Earth and Planetary Science Letters 277 (1), 262.

Shaked, Y., Xu, Y., Leblanc, K., Morel, F.M.M., 2006. Zinc availability and alkaline phosphatase activity in Emiliania huxleyi: Implications for Zn-P co-limitation in the ocean. Limnology and Oceanography 51 (1), 299–309.

Sherrell, R.M., Lagerström, M.E., Forsch, K.O., Stammerjohn, S.E., Yager, P.L., 2015. Dynamics of dissolved iron and other bioactive trace metals (Mn, Ni, Cu, Zn) in the Amundsen Sea Polynya. Antarctica. Elementa: Science of the Anthropocene 3, 000071.

Sieber, M., Conway, T.M., de Souza, G.F., Hassler, C.S., Ellwood, M.J., Vance, D., 2019. High-resolution Cd isotope systematics in multiple zones of the Southern Ocean from the Antarctic Circumnavigation Expedition. Earth and Planetary Science Letters 527, 115799.

Sieber, M., Conway, T.M., de Souza, G.F., Hassler, C.S., Ellwood, M.J., Vance, D., 2020. Cycling of zinc and its isotopes across multiple zones of the Southern Ocean: Insights from the Antarctic Circumnavigation Expedition. Geochimica et Cosmochimica Acta 268, 310–324.

Sieber, M., Conway, T.M., de Souza, G.F., Obata, H., Takano, S., Sohrin, Y., Vance, D., 2019. Physical and biogeochemical controls on the distribution of dissolved cadmium and its isotopes in the Southwest Pacific Ocean. Chemical Geology 511, 494–509.

Sieber, M., Lanning, N.T., Bian, X., Yang, S.C., Takano, S., Sohrin, Y., Weber, T.S., Fitzsimmons, J.N., John, S.G., Conway, T.M., 2023. The Importance of Reversible Scavenging for the Marine Zn Cycle Evidenced by the Distribution of Zinc and Its Isotopes in the Pacific Ocean. Journal of Geophysical Research: Oceans 128 (4), e2022JC019419.

Sieber, M., Lanning, N.T., Bunnell, Z.B., Bian, X., Yang, S.-C., Marsay, C.M., Landing, W. M., Buck, C.S., Fitzsimmons, J.N., John, S.G., Conway, T.M., 2023. Biological, Physical, and Atmospheric Controls on the Distribution of Cadmium and Its Isotopes in the Pacific Ocean. Global Biogeochemical Cycles 37 (2), e2022GB007441.

Siebert, C., Nägler, T.F., Kramers, J.D., 2001. Determination of molybdenum isotope fractionation by double-spike multicollector inductively coupled plasma mass spectrometry. Geochemistry, Geophysics, Geosystems 2 (7), 1032.

Sunda, W.G., Huntsman, S.A., 1995. Cobalt and zinc interreplacement in marine phytoplankton: Biological and geochemical implications. Limnology and Oceanography 40 (8), 1404–1417.

Takano, S., Tanimizu, M., Hirata, T., Shin, K.-C., Fukami, Y., Suzuki, K., Sohrin, Y., 2017. A simple and rapid method for isotopic analysis of nickel, copper, and zinc in seawater using chelating extraction and anion exchange. Analytica Chimica Acta 967, 1–11.

Tian, H.-A., van Manen, M., Bunnell, Z.B., Jung, J., Lee, S.H., Kim, T.-W., Reichart, G.-J., Conway, T.M., Middag, R., 2023. Biogeochemistry of iron in coastal Antarctica: isotopic insights for external sources and biological uptake in the Amundsen Sea polynyas. Geochimica et Cosmochimica Acta 363, 51–67.

Tian, H.-A., van Manen, M., Wille, F., Jung, J., Lee, S., Kim, T.-W., Aoki, S., Eich, C., Brussaard, C.P.D., Reichart, G.-J., Conway, T.M., Middag, R., 2023. The biogeochemistry of zinc and cadmium in the Amundsen Sea, coastal Antarctica. Marine Chemistry 249, 104223.

Twining, B.S., Baines, S.B., 2013. The Trace Metal Composition of Marine Phytoplankton. Annual Review of Marine Science 5 (1), 191–215.

Twining, B.S., Baines, S.B., Fisher, N.S., 2004. Element stoichiometries of individual plankton cells collected during the Southern Ocean Iron Experiment (SOFeX). Limnology and Oceanography 49 (6), 2115–2128.

Twining, B.S., Baines, S.B., Fisher, N.S., Maser, J., Vogt, S., Jacobsen, C., Tovar-Sanchez, A., Sañudo-Wilhelmy, S.A., 2003. Quantifying Trace Elements in Individual Aquatic Protist Cells with a Synchrotron X-ray Fluorescence Microprobe. Analytical Chemistry 75 (15), 3806–3816.

van Leeuwe, M.A., Villerius, L.A., Roggeveld, J., Visser, R.J.W., Stefels, J., 2006. An optimized method for automated analysis of algal pigments by HPLC. Marine Chemistry 102 (3), 267–275.

van Manen, M., Aoki, S., Brussaard, C.P.D., Conway, T.M., Eich, C., Gerringa, L.J.A., Jung, J., Kim, T.-W., Lee, S., Lee, Y., Reichart, G.-J., Tian, H.-A., Wille, F., Middag, R., 2022. The role of the Dotson Ice Shelf and Circumpolar Deep Water as driver and source of dissolved and particulate iron and manganese in the Amundsen Sea polynya. Southern Ocean. Marine Chemistry 246, 104161.

Vance, D., de Souza, G.F., Zhao, Y., Cullen, J.T., Lohan, M.C., 2019. The relationship between zinc, its isotopes, and the major nutrients in the North-East Pacific. Earth and Planetary Science Letters 525, 115748.

Vance, D., Little, S.H., de Souza, G.F., Khatiwala, S., Lohan, M.C., Middag, R., 2017. Silicon and zinc biogeochemical cycles coupled through the Southern Ocean. Nature Geoscience 10 (3), 202–206.

Vernet, M., Geibert, W., Hoppema, M., Brown, P.J., Haas, C., Hellmer, H.H., Jokat, W., Jullion, L., Mazloff, M., Bakker, D.C.E., Brearley, J.A., Croot, P., Hattermann, T., Hauck, J., Hillenbrand, C.D., Hoppe, C.J.M., Huhn, O., Koch, B.P., Lechtenfeld, O.J., Meredith, M.P., Naveira Garabato, A.C., Nöthig, E.M., Peeken, I., Rutgers van der Loeff, M.M., Schmidtko, S., Schröder, M., Strass, V.H., Torres-Valdés, S., Verdy, A., 2019. The Weddell Gyre, Southern Ocean: Present Knowledge and Future Challenges. Reviews of Geophysics 57 (3), 623–708.

Wåhlin, A.K., Kalén, O., Arneborg, L., Björk, G., Carvajal, G.K., Ha, H.K., Kim, T.W., Lee, S.H., Lee, J.H., Stranne, C., 2013. Variability of Warm Deep Water Inflow in a Submarine Trough on the Amundsen Sea Shelf. Journal of Physical Oceanography 43 (10), 2054–2070.

Wang, R.M., Archer, C., Bowie, A.R., Vance, D., 2019. Zinc and nickel isotopes in seawater from the Indian Sector of the Southern Ocean: The impact of natural iron fertilization versus Southern Ocean hydrography and biogeochemistry. Chemical Geology 511, 452–464.

Weber, T., John, S., Tagliabue, A., DeVries, T., 2018. Biological uptake and reversible scavenging of zinc in the global ocean. Science 361 (6397), 72.

Westerlund, S., öhman, 1991. Cadmium, copper, cobalt, nickel, lead, and zinc in the water column of the Weddell Sea. Antarctica. Geochimica et Cosmochimica Acta 55 (8), 2127–2146.

Xie, R.C., Galer, S.J.G., Abouchami, W., Rijkenberg, M.J.A., de Baar, H.J.W., De Jong, J., Andreae, M.O., 2017. Non-Rayleigh control of upper-ocean Cd isotope fractionation in the western South Atlantic. Earth and Planetary Science Letters 471, 94–103.

Xie, R.C., Rehkämper, M., Grasse, P., van de Flierdt, T., Frank, M., Xue, Z., 2019. Isotopic evidence for complex biogeochemical cycling of Cd in the eastern tropical South Pacific. Earth and Planetary Science Letters 512, 134–146.

Xue, Z., Rehkämper, M., Horner, T.J., Abouchami, W., Middag, R., van de Flierd, T., de Baar, H.J.W., 2013. Cadmium isotope variations in the Southern Ocean. Earth and Planetary Science Letters 382, 161–172.

Yager, P.L., Sherrell, R.M., Stammerjohn, S.E., Alderkamp, A.-C., Schofield, O., Abrahamsen, E.P., Arrigo, K.R., Bertilsson, S., Garay, D.L., Guerrero, R., Lowry, K.E., Moksnes, P.-O., Ndungu, K., Post, A.F., Randall-Goodwin, E., Riemann, L., Severmann, S., Thatje, S., Van Dijken, G.L., Wilson, S., 2012. ASPIRE: The Amundsen Sea Polynya International Research Expedition. Oceanography 25 (3), 40–53.

Yang, S.-C., Lee, D.-C., Ho, T.-Y., 2012. The isotopic composition of Cadmium in the water column of the South China Sea. Geochimica et Cosmochimica Acta 98, 66–77.

Yang, S.-C., Lee, D.-C., Ho, T.-Y., 2015. Cd isotopic composition in the suspended and sinking particles of the surface water of the South China Sea: The effects of biotic activities. Earth and Planetary Science Letters 428, 63–72.

Yang, S.-C., Zhang, J., Sohrin, Y., Ho, T.-Y., 2018. Cadmium cycling in the water column of the Kuroshio-Oyashio Extension region: Insights from dissolved and particulate isotopic composition. Geochimica et Cosmochimica Acta 233, 66–80.

Zhao, Y., Vance, D., Abouchami, W., de Baar, H.J.W., 2014. Biogeochemical cycling of zinc and its isotopes in the Southern Ocean. Geochimica et Cosmochimica Acta 125, 653–672.